CAL-1811R

(2)

FINAL TECHNICAL REPORT FOR OFFICE OF NAVAL RESEARCH CONTRACTS N00014-83-K-0494 AND N00014-86-C-0086

Title of Research: **"Development of Liquid Xenon Imaging Gamma-Ray Spectrophotometers"**

Principal Investigators: Robert Novick
Professor of Physics

and

Elena Aprile
Associate Professor of Physics

Prepared by: Columbia Astrophysics Laboratory
538 West 120th Street
New York, NY 10027

Contract Number: ONR N 00014-83-K-0494

Period of Research: 1 June 1983 – 30 November 1985

and

Contract Number: ONR N 00014-86-C-0086

Period of Research: 1 December 1985 – 30 November 1989

"The views and conclusions contained in this document are those of the authors and should not be interpreted as necessarily representing the official policies, either expressed or implied, of the Defense Advanced Research Projects Agency or the U.S. Government."

July 1990

Unclassified

SECURITY CLASSIFICATION OF THIS PAGE

REPORT DOCUMENTATION PAGE

Form Approved OMB No. 0704-0188

1a. REPORT SECURITY CLASSIFICATION: Unclassified	1b. RESTRICTIVE MARKINGS
2a. SECURITY CLASSIFICATION AUTHORITY: ---	3. DISTRIBUTION/AVAILABILITY OF REPORT: Approved for Public Release
2b. DECLASSIFICATION/DOWNGRADING SCHEDULE: ---	
4. PERFORMING ORGANIZATION REPORT NUMBER(S): CAL - 1811R	5. MONITORING ORGANIZATION REPORT NUMBER(S)
6a. NAME OF PERFORMING ORGANIZATION: Columbia University; 6b. OFFICE SYMBOL (If applicable)	7a. NAME OF MONITORING ORGANIZATION: Office of Naval Research
6c. ADDRESS (City, State, and ZIP Code): Box 20 Low Memorial Library, New York, NY 10027	7b. ADDRESS (City, State, and ZIP Code): 800 N. Quincy St. (Code 1114SP), Arlington, VA 22217
8a. NAME OF FUNDING/SPONSORING ORGANIZATION: Defense Advance Research Projects Agency; 8b. OFFICE SYMBOL (If applicable): NMRO	9. PROCUREMENT INSTRUMENT IDENTIFICATION NUMBER: N00014-83-K-0494, N00014-86-C-0086
8c. ADDRESS (City, State, and ZIP Code): 1400 Wilson Blvd., Arlington, VA 22209-2308	10. SOURCE OF FUNDING NUMBERS: PROGRAM ELEMENT NO. 62714E; PROJECT NO. 7A10; TASK NO. 4349; WORK UNIT ACCESSION NO. jd 14002

11. TITLE (Include Security Classification)

(U) Final Technical Report for ONR Contracts N00014-83-K0494 and N00014-86-C-0086

12. PERSONAL AUTHOR(S): Robert Novick and Elena Aprile

13a. TYPE OF REPORT	13b. TIME COVERED	14. DATE OF REPORT (Year, Month, Day)	15. PAGE COUNT
Final Technical	FROM 1June83 TO30Nov89	1990, July	---

16. SUPPLEMENTARY NOTATION: N.A.

17. COSATI CODES		
FIELD	GROUP	SUB-GROUP

18. SUBJECT TERMS (Continue on reverse if necessary and identify by block number): Liquid Xenon Imaging Gamma-Ray Spetrophotometers

19. ABSTRACT (Continue on reverse if necessary and identify by block number)

(U) We have investigated the application of liquid xenon in high resolution, low background and efficient γ ray detectors for the observation in space of weak sources emitting in the 0.1 – 10 MeV energy region.

The basic requirement of ultra-high purity liquid xenon, necessary for the successful operation of these detectors has been satisfied with the development of an efficient and reliable purification system, capable of reducing and maintaining the concentration of electronegative impurities below one part in 10^9.

The charge and energy resolution response of a liquid xenon (and liquid argon) ionization chamber has been systematically measured as a function of electric field strength, using various radioactive sources. Our results of 4.5% FWHM and 2.6% FWHM at 1 MeV in liquid xenon and liquid argon, respectively are the best reported in the literature. Their deviation from theoretical estimates based on Fano factor statistics has been interpreted as due to recombination straggling on low energy δ electrons produced along the primary ionizing particle.

(Over)

20. DISTRIBUTION/AVAILABILITY OF ABSTRACT	21. ABSTRACT SECURITY CLASSIFICATION
☐ UNCLASSIFIED/UNLIMITED ☒ SAME AS RPT ☐ DTIC USERS	UNCLASSIFIED
22a. NAME OF RESPONSIBLE INDIVIDUAL: R.G. Joiner	22b. TELEPHONE (Include Area Code): (202) 696-4203; 22c. OFFICE SYMBOL: ONR Code 114SP

DD Form 1473, JUN 86 Previous editions are obsolete. SECURITY CLASSIFICATION OF THIS PAGE

19. ABSTRACT. *(Continued)*

(U)

The effect of photosensitive dopants in the liquid has also been measured. Improved charge collection and energy resolution is observed for the case of alpha particles.

In view of its application for event triggering in an imaging ionization chamber, we have measured the yield of the primary scintillation light abundantly emitted in liquid xenon, using both electrons and alpha particles. The dependence of the light signal on the ionization density of the event will provide an ideal tool for background rejection.

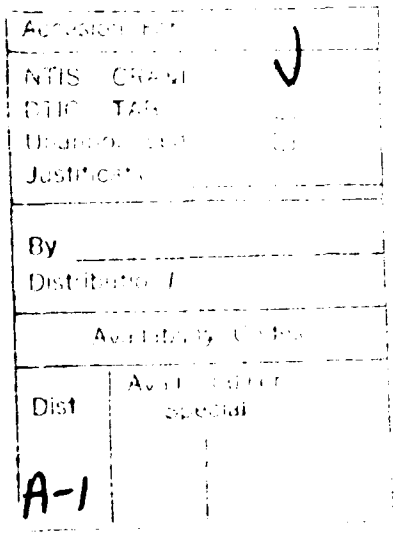

Final Technical Report for ONR Contracts N00014-83-K-0494 and N00014-86-C-0086

The objective of this project was to develop advanced imaging X-ray and γ-ray spectrometers, based on the use of liquid rare gases, xenon in particular. These detectors will have important applications in space based detection of weak γ-ray sources, with orders of magnitude improved sensitivity over more common NaI(Tℓ) or Ge(Li) spectrophotometers.

The unique properties of liquid xenon as detector medium, especially for X-rays include:

- High detection efficiency for e^- and γ, similar to that of NaI(Tℓ), due to the high atomic number ($Z = 54$) and density ($\rho = 3$ g cm^{-3}).
- Excellent energy resolution, theoretically similar to that of Ge, due to the small Fano factor ($F = 0.04$) and average energy to create an electron-ion pair ($W = 15.6eV$).
- Excellent spatial resolution, due to the small electron diffusion, with the possibility of a complete three-dimensional event imaging in a Time Projection type Chamber triggered by the fast scintillation.
- Excellent scintillation efficiency, comparable to that of NaI(Tℓ) and with a fast decay time.
- Effective background rejection capability, as direct consequence of imaging.

Among the technical problems which have challenged the realization of a liquid xenon instrument with high resolution, imaging capability, and large sensitive area are:

- Achieve and maintain a high level of purity for the liquid xenon with less than 1 ppb (1 part per billion) contamination of oxygen-like substances.

- Limited choice of construction materials satisfying both the requirements of extremely low outgas and cryogenic operation.
- Complexity of a position sensitive readout system capable of submillimeter spatial resolution, with the requirement of low noise electronics for a large number of channels and in the presence of high voltages.

We have extensively studied the fundamental properties of liquid rare gas ionization and scintillation detectors. Important experimental results with both liquid argon and liquid xenon, especially in the areas of gas purification, ionization and scintillation yields of different radiations as well as in the areas of spectral resolution, have been achieved during the period of the contracts.

In the following we summarize the laboratory experiments and results, with reference to the published literature for further details, and indication for further studies and research.

1.0. The Liquid Xenon Proportional Scintillation Chamber Approach

During the initial phase of ONR contract N00014-83-K-0494 we concentrated our efforts to the design, construction and test of a prototype liquid xenon chamber which could be used both in ionization and scintillation modes, with an emphasis on proportional scintillation. The basic advantage of this mode of detector operation is represented by the large increase in available signal, compared to the ionization mode, with however similarly excellent spectral resolution.

1.1. Detector Design

Figure 1 shows the first liquid xenon prototype developed at Columbia, using the successful design of the imaging gas scintillation proportional counter (IGSPC).

A pill-box shaped cell, filled with high purity xenon, absorbs incident γ-rays entering through a 250μm thick stainless steel (SS) window and converts each one into several tens of thousands of UV photons and primary electron-ion pairs. The

electrons drift in a 7.5mm deep region defined by the SS entrance window held at ground potential and a 85% transparent, SS etched mesh held at $V_c \sim 1$kV toward a high field region. The electrons are accelerated in the high field regions surrounding a 5cm diameter plane of 10μm diameter gold-plated tungsten anode wires spaced 2mm apart and held at a potential of V_a. They gain sufficient energy to excite other xenon atoms to emit UV photons. A second SS mesh defines the bottom of the $\pm$5mm deep excitation region. The electrons are collected on the thin anode wires and processed by a charge-sensitive preamplifier. The photons escape through two UV transparent, 10cm diameter, quartz windows and are absorbed in a second stage detector – a photomultiplier tube (PMT) or a multiwire proportional counter (MWPC) filled with tetrakis (dimethylamino) ethlene (TMAE) and argon gas.

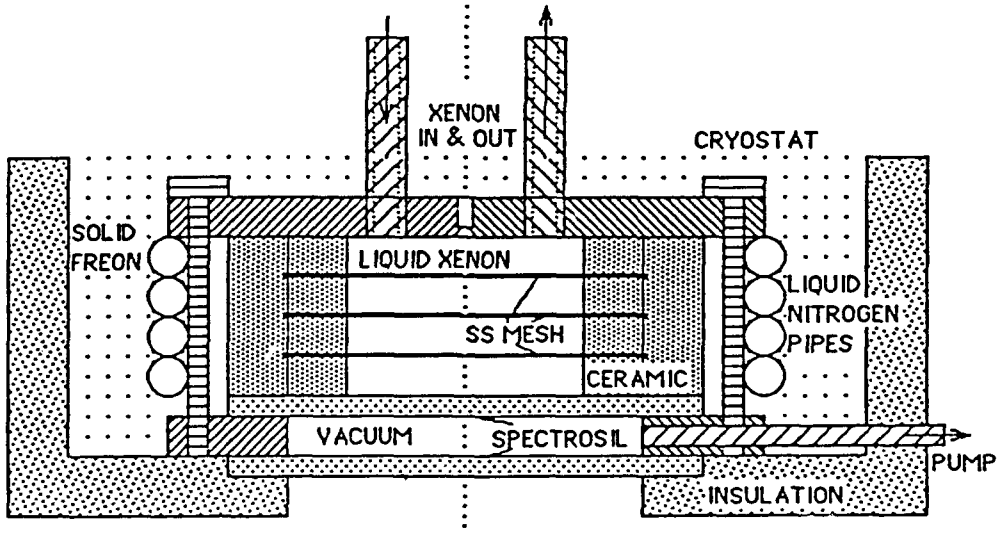

Figure 1. Schematic of the liquid xenon test cell.

The lower quartz disk also forms the window for the MWPC below (Fig. 2). The MWPC is a $20 \times 20 \times 2.5$cm aluminum box filled with TMAE, plus argon and a quench gas. Each UV photon ejects a photoelectron from a TMAE molecule. These electrons drift in a low field region defined by a grounded SS mesh located on the lower surface of the calcium flouride window and a cathode wire plane located 11mm below, held at ground potential. The cathode plane is made from 63μm diameter silver-plated berylliun copper wire set at 0.55mm pitch on a 15cm span. These wires are grouped together into 20 sets of 14 wires each. The photoelectrons are accelerated through the cathode plane toward a HV anode plane located 6mm away. The anode wire plane is made from 20μm diameter gold-plated tungsten wire set at 2mm pitch. A lower cathode plane, with wires set orthogonal to the wires on the upper cathode plane, defines a total active region of 23mm depth. The avalanching electrons are collected on the anode wires while the ions are collected on the cathode wires. Large charge pulses are induced on the crossed cathode planes. Spatial information is obtained by calculating the two-dimensional centroid of the charge distribution sensed by the grouped cathode wires. Energy information may be obtained by collecting the electrons in a charge sensitive preamplifier attached to the anode plane or by summing the cathode signals.

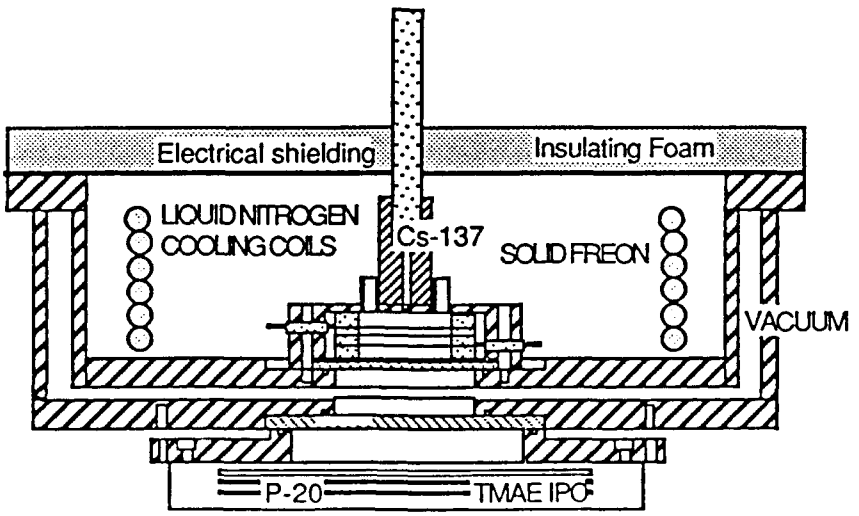

Figure 2. A scaled diagram of the prototype imaging liquid xenon counter - shown with a TMAE MWPC as the second stage detector. Alternatively a PMT may be used.

Since at 1 atm the liquid phase of xenon extends from approximately 162K to 165K (see Fig. 3), a precise temperature controlled cooling unit is necessary. The cooling system designed and tested for the first LXe prototype is shown in Fig. 2.

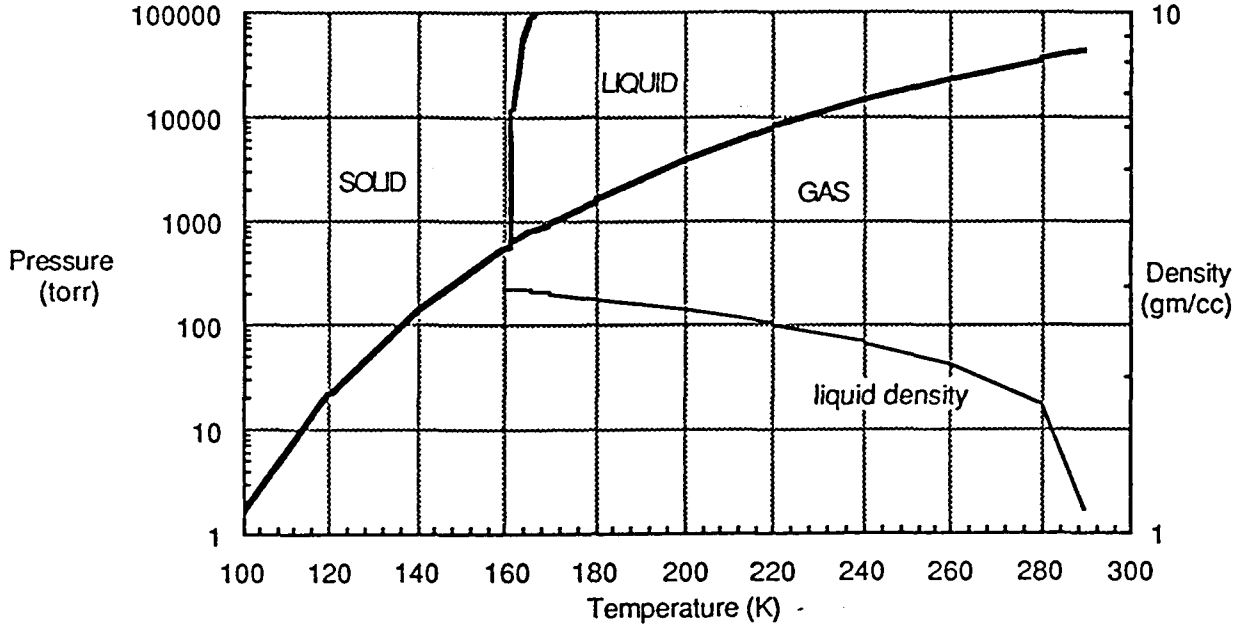

Figure 3. Pressure and density (liquid) versus temperature plot for xenon. Triple Point temperature = 161.391K, pressure = 612.2 torr, density (liquid) = 2.96 gm/cm^3, and density (gas) = 8.18 mg/cm^3.

The front cell is surrounded by a freon bath which is cooled and solidified by liquid nitrogen, and thermally isolated from the outside world by a vacuum insulation layer. Solid freon gives a convenient and accurate way of maintaining the liquid xenon at 162K, but requires extreme care in insuring the vacuum integrity of the liquid xenon cell, since freon is extremely electronegative. The freon is kept in a 30cm diameter by 10cm deep SS cryostat large enough to accomodate a 15cm diameter by 5cm deep liquid xenon cell and copper cooling coils circulating liquid nitrogen. An aluminum plate and styrofoam layer electrically isolates and thermally insulates the top of the cryostat. A radioactive source can be inserted through the top insulation to ascertain the detection of γ-rays and removed to check the background level. Temperature sensors outside, and pressure sensors inside the xenon cell monitor the thermodynamic state of the xenon. A Macintosh microcomputer monitors these temperatures and pressures, and operates the solenoid valves which

control the liquid nitrogen level and flow rate.

1.2. Electronics

Three low-noise, charge-sensitive preamplifiers are used to process the charge signals from the xenon test cell: one each attached to the front cathode, anode, and back cathode planes. The preamplifiers are located some distance from the counter and suffer from $\sim 2000e^-$ (FWHM) of noise. Charge signals are operated in coincidence with each other and the signal from the second stage to minimize spurious background events. Each of the signals is then passed into a pulse shape analyzer which outputs a voltage signal proportional to the signal rise times. The pulse height and rise time information are then passed into analog to digital convertors (ADC) which displays the spectra.

A voltage amplifier processes the signal from the high-gain, UV sensitive PMT, initially used as second stage detector.

1.3. Purification System

An important prerequisite for the devlopment of a liquid rare gas detector, aiming at good energy and spatial resolution, is the ultra high purity of the liquid. A total concentration below few parts per billion (ppb) of electronegative impurities, such as O_2, CO_2, CO, H_2O, hydrocarbons and fluorocarbons, is required to minimize the capture probability of free conduction electrons, with consequent reduction of the total charge signal and hence resolution. For the detection of a scintillation signal in liquid rare gases, the purity of the liquid is less critical although substantial absorption of the UV light is expected for concentrations of complex compounds, expecially hydrocarbons, at the level of several hundreds of ppb.

The purification system that was developed for the liquid xenon proportional scintillation counter is shown in Fig. 4.

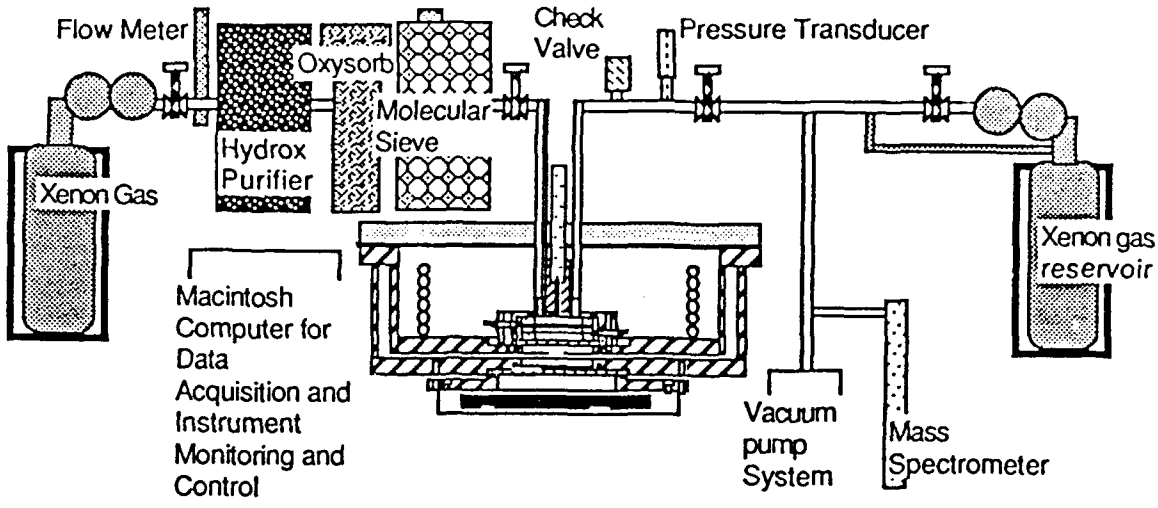

Figure 4. A scaled diagram of the prototype imaging liquid xenon counter, shown with complete liquefaction and purification system.

1.4. Results

Many parameters of this first liquid xenon prototype were tested initially using a 1 – 3 atm of xenon gas. At low high voltages, $\sim$ 1kV, the PMT detected a weak light signal with $\sim$ 100ns rise time corresponding to primary scintillation photons. We estimate that geometric factors (16%Ω = 1.1sr), quartz windows (36% = 0.6 $\times$ 0.6), and photocathode efficiencies (20%) yield a net efficiency of $\sim$ 1% – i.e. $\sim$ 5 UV photons for each 11.5 keV depositied in the xenon gas. As we increased the HV, we began to detect secondary scintillation photons with $\sim 2\mu$s rise times. The light gain increased with HV. At even higher HV, we detected an electron signal with $\sim 2\mu$s rise times. The charge gain increases exponentially with HV.

A typical electron pulse height spectrum obtained by a counter filled with 3 atm of xenon tested with a ^{153}Cd radioactive source is shown in Figure 5. The energy resolutions obtained, 28% (FWHM) for the 11.5 keV line, is worse than typical proportional counter resolutions due to imperfections in the HV grids, poor

collimation of the γ-rays, and the lack of a sufficiently deep absorption-drift region. The light signal from the PMT yielded very similar spectrum with somewhat better energy resolutions at lower HV where charge gain fluctuations are less important. Depending on the purity of the gas and cleaniness of the detector cell, the charge gain degraded $\sim 5\% - 30\%$ per day.

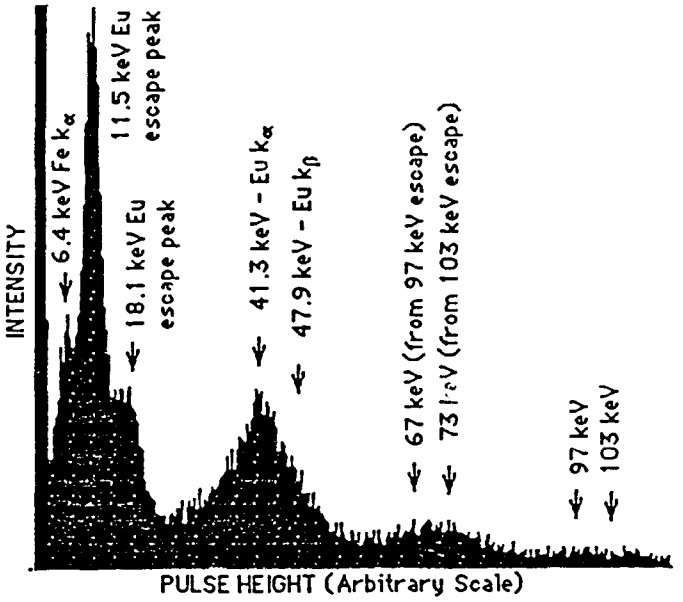

Figure 5. Pulse height spectrum recorded for γ-ray photons from a ^{135}Gd radioactive source absorbed by 3-atm of xenon.

Results obtained with a ^{137}Cs radioactive source in the liquid xenon counter operated in the ionization and scintillation modes are shown in Fig. 6.

Operating with $V_a \sim 1$kV we detected fast rising (~ 100 ns) primary scintillation photons with a high gain PMT (Fig. 6). However, the signals we detected were much lower, and the energy resolution much worse, than what we expected. 662 keV γ-rays from a ^{137}Cs radioactive source should produce 42,000 electron-ion pairs and a similar number of UV photons in liquid xenon. The xenon gas measurements suggest that we should be able to detect these 662 γ-rays with $\sim 20\%$ (FWHM) resolution. However, we could not resolve this line above the Compton continuum and background. The approximately exponential spectra we measured correspond to $\sim 100\%$ (FWHM) energy resolution (Fig. 6). At higher HV, $V_a \sim 4$kV, we de-

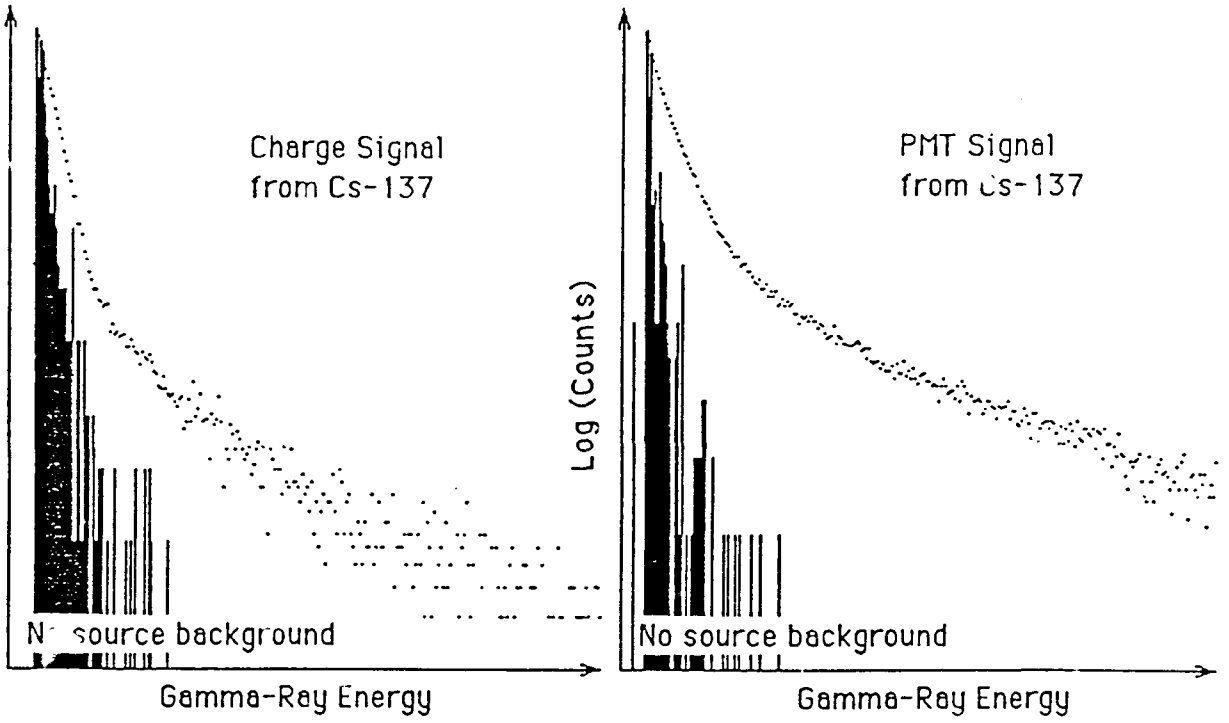

Figure 6. Pulse height response of liquid xenon detector to γ-rays from ^{137}Cs radioactive source. The pulse height spectrum from the charge preamplifier for source compared with no source is shown on the left; the pulse height spectrum from the PMT for source compared with no source is shown on the right.

tected a larger amplitude, slower rising ($\sim 2\mu$s) light signal and a significant charge signal. Unfortunately, the energy resolution of the light signal did not improve with increased HV. The charge signal, while 10 times higher than the electronic noise level of $\sim 2000e^-$ (FWHM), did not yield any better energy resolution. We calculate that we should detect 662 keV photons with 6% (FWHM) energy resolution. We observed exponential spectra with a maximum pulse height equal to, but often less than half of what we expected. At $V_a \leq 5$kV, the counter failed to operate reliably with the 10μm tungsten anode wires breaking quite often.

Two main reasons have been responsible for the poor performance of this first prototype liquid xenon proportional counter.

The first is associated to inadequate purification of the liquid xenon, coupled with the technical problem of reliable seals between the quartz windows and the

SS detector body. Substantial deterioration of the liquid purity was caused by temperature-dependent leaks in the detector, due to the failure of the indium seal used between SS and quartz. The presence of even a tiny leak during the detector cooling from room temperature to $\sim$ 162K has an enormous effect on the performance given the highly electronegative freon bath used.

The second critical element in this initial development is associated with the electric field geometry and electrical breakdown due to surface irregularities on the HV grid wires. The anode grids, made individually by hand, had to satisfy many requirements, often conflicting with each other. They had to be made strong enough to withstand electrostatic stress and multiple thermal cycles. In addition, the wire spacing had to be extremely uniform to insure uniform light and charge collection.

These and other technical challenges experienced in the first phase of the project resulted however into an important learning process which culminated with the improved chamber designs and xenon purification system developed during the second phase of the development.

2.0. The Liquid Xenon Imaging Ionization Chamber Approach

During the second phase of the project under ONR contract N00014-86-C-0086 we worked on finding appropriate solutions to the technical problems experienced in the first period, especially with respect to effective purification methods for xenon and to chamber stability under high voltages.

Further, we initiated systematic studies of the basic properties of liquid xenon, using both its characteristics as ionization material and as fast scintillator. These studies have led us to the choice of a liquid xenon imaging chamber operated in the ionization mode, triggered by the scintillation light, to provide both the energy of the incident radiation with excellent resolution, as well as the incident direction with accurate angular resolution.

Experimental results in both liquid argon and xenon have been published in refereed journals and presented at several international conferences. In the following

we will summarize these developments, for a more detailed description we refer to the articles attached with this final report.

2.1. Detector Design

Several prototype liquid xenon ionization chambers were built and tested during this period, using various radioactive sources or cosmic rays.

Figure 7 shows a typical gridded type ionization chamber designed for studies of ionization yield and energy resolution of electrons and gamma-rays in liquid xenon. Two solid SS disks form the cathode and anode. An electroformed nickel mesh is used as screening grid, below the anode. For measurements with α-particles, a parallel plate configuration was used. Details of this chamber design can be found in references [1,2].

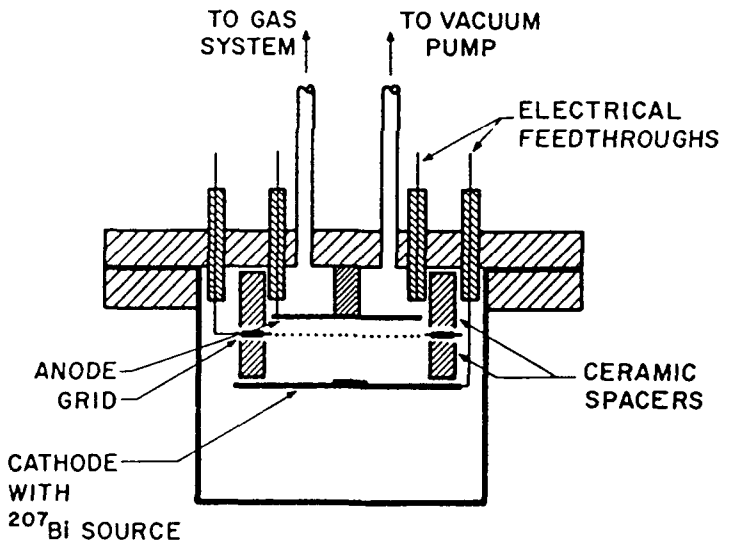

Figure 7. Schematic cross section of the gridded ionization chamber.

Gamma-rays interacting with the sensitivie volume of the chamber produce secondary particles by photoabsorption, Compton scattering, or pair production. These charged particles will dissipate their energy by ionization and excitation of the liquid xenon, creating a large number of electron-ion pairs along their trajectory,

as well as scintillation photons. Under the influence of an external electric field, the ionization electrons which escape recombination with the positive ions and which are not trapped by impurities will drift from their point of creation towards the anode. The total ionizing event can be measured from the induced charge signal on the collector. For the signal to be truly proportional to the total energy of the ionizing event, a shielding grid is necessary. To obtain also the spatial development of the event, the anode can be substituted with a complex structure of orthagonal wire planes or, more simply with a segmented anode.

The X and Y information is extracted from the location of the induced signals on the sensing elements. The third coordinate, parallel to the electric field, is deduced with the known electron drift velocity from the measured drift time, as referenced to the event starting time t_0. Thus a complete 3-dimensional event image is realized.

Since liquid xenon is an excellent scintillator, the detection of the primary scintillation light with its fast decay constant, can be used to indicate the start time t_0 of an event.

2.2. Xenon Purification System and Purity Monitor

Impurities in the filling liquid come generally from the gas composition itself, from outgassing of materials and from external leaks. An efficient gas handling/purification system designed according to high vacuum standards and the choice of "clean" bakeable materials is a necessary prerequisite for the successful operation of a liquid ionization chamber. A total concentration of impurities as low as a few parts per billion (ppb) is required to keep the ionization electrons free to drift over large distances under the effect of an external field. We have tested different purification techniques, combining both active and passive absorbers. The system shown in Fig. 8 was designed and tested to give consistently less than 1 ppb O_2 equivalent impurities concentration in liquid argon (LAr). We used LAr in the initial phase of the purifications tests because of its much better known physical

properties in comparison with liquid xenon (LXe) and its cheaper cost. An analysis of the pulse shape of the ionization signals induced by cosmic rays in LAr, yields directly the purity level of less than 1 ppb. The application of the same system to the purification of xenon resulted to be not adequate to yield the desired purity level. Compared to argon, xenon is much more difficult to purify. The oxygen attachment cross section in LXe is higher than in LAr and the higher temperature of $\sim$ 162 K at 1 atm as compared to $\sim$ 87 K for LAr allows more impurities to be in solution. It is, however, the removal of non-oxygen like substances which represents the most serious challenge in the xenon purification, especially since their attachment probability is found to increase with increasing drift field strength. The purification system was modified for the xenon operation and the set-up is shown in Fig. 9.

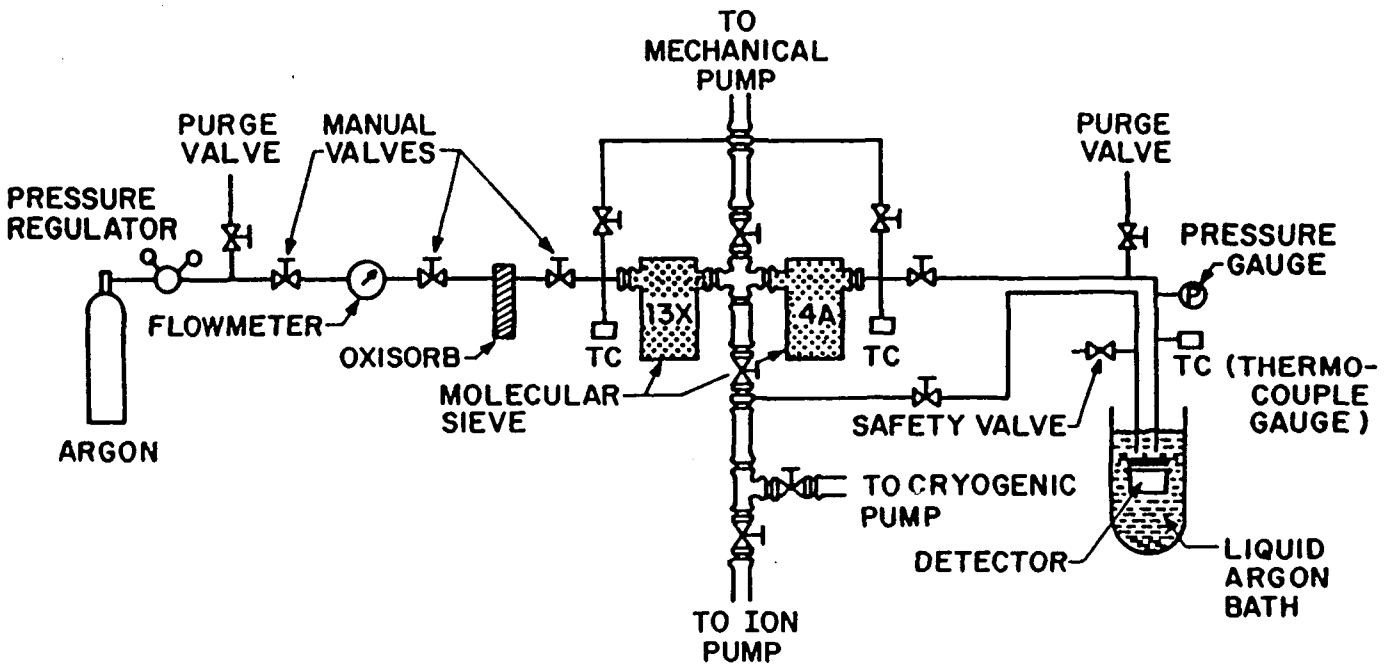

Figure 8. Schematic drawing of the gas handling and purification system for LAr.

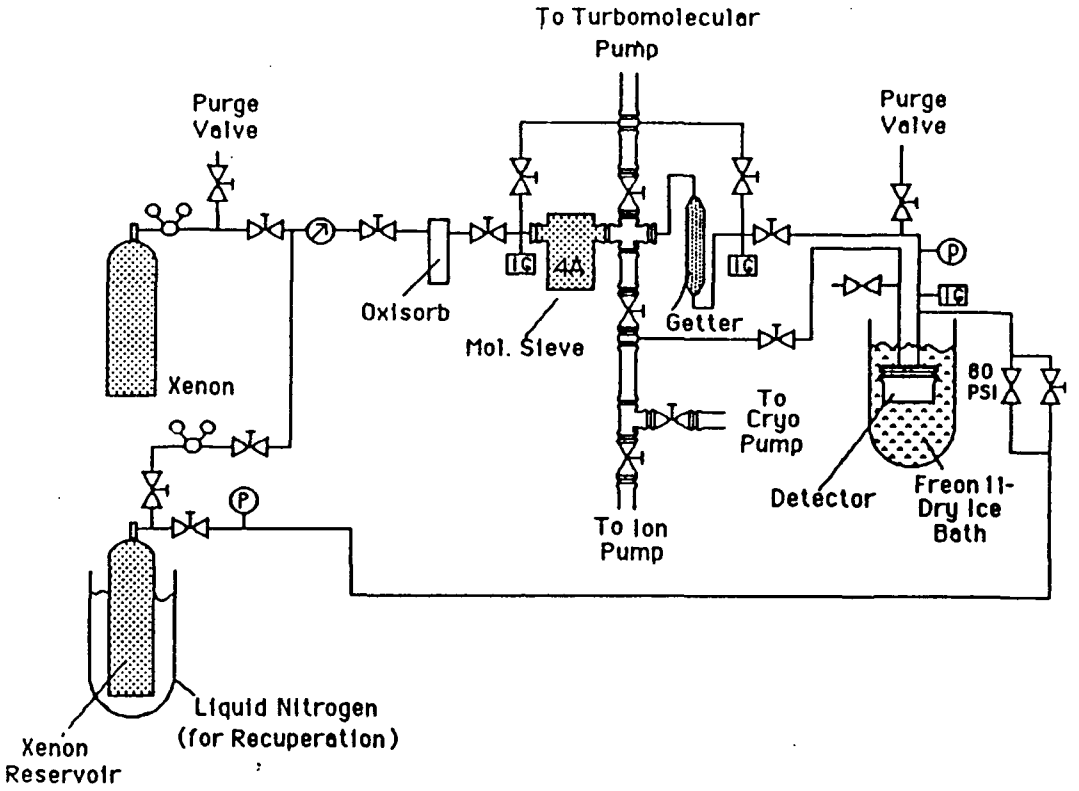

Figure 9. Schematic drawing of the gas handling and purification system for LXe.

The commercial xenon gas used was the research grade type with the following impurity specification: $H_2O < 0.5$ ppm, $O_2 < 1.0$ ppm, $C_nH_m < 0.5$ ppm, $N_2 < 3.0$ ppm, Kr < 15 ppm, $CO_2 < 1.0$ ppm and $H_2 < 2.0$ ppm, where ppm stands for parts per million. From the standard gas bottles, the xenon was transferred into a stainless stell high pressure cylinder. With a volume of 3.78 liters, the cylinder contained the xenon gas with a pressure of 54 atm, corresponding to 620 cm^3 of liquid. Before storing the gas, the reservoir was ultrasonically cleaned, evacuated and baked at 200°C for 24 hours. The ultimate outgas rate of the reservoir was better than 1.0×10^{-9} torr · liter/sec.

The xenon gas was purified in the following sequence. First it was passed through a commercial oxisorb, to remove the buk of oxygen below 0.1 ppm by chemisorption on a highly active metallic surface. The oxisorb also reduces water to less than 0.5 ppm.

From the oxisorb the gas is passed through a molecular sieve trap filled with approximately one kilogram of 4A type synthetic zeolites, in the form of pellets. The action of this passive adsorber is to remove molecules with an effective diameter less than 4 angstroms, including water, CO_2 and light hydrocarbons. We purposely renounced the use of 13X type molecular sieves because of the substantial adsorption of xenon gas, in this size zeolites (about 200 g/l kg of sieves at 1 atm and 25°C). The sieve trap was operated at room temperature. The last stage of purification was performed with two high temperature getters. The first getter uses an alloy of (Zr-V-Fe) and active elements. Among the impurities removed are: H_2O, H_2, O_2, N_2, CO, CO_2, CH_4, NO_x, NH_3, CF_4, $CC\ell$, SiH_4 and light hydrocarbons. The second getter containing an alloy of (Zr-Fe), is used to remove H_2 which may diffuse out from the first getter.

The gas system did not include a continuous circulation of the gas through the purifiers. We found that approximately four cycles of purification with the sequence described above, were necessary to clean the gas to the desired level.

The purification system along with the gas filling and recuperation lines, was built with stainless stell tubing and the connections were either welded or made with high vacuum fittings. The valves used were all metal, bakeable ones.

After initial cleaning and assembly, the system was baked under vacuum for several weeks and was always kept under vacuum between each measurement, except for the oxisorb which was kept under xenon pressure. To activate the molecular sieve trap, after the initial filling with the pelletts, a temperature of 350°C under a good vacuum was maintained for several weeks. In between runs the sieve trap was regenerated by baking at 350°C for 72 hours under a vacuum of 10^{-7} torr.

Before each gas filling, both getters were activated at 350°C for 2 hours. After the activation, the first and the second getter were maintained at the operational temperature of 500°C and 150°C, respectively for the whole period of detector filling.

Typical outgassing rate of the system and the chamber was better than 10^{-8}

torr · liter/sec.

After purification as described above, the xenon gas was liquefied in the chamber by surrounding it with an open bath of Freon-11 at dry ice temperature (195 K). This choice provided a practical and reliable way to maintain a constant liquid xenon temperature. Since the vapor pressure of xenon at dry-ice temperature is about 4 atm, the pressure of the gas has to exceed this value to condense. We passed the gas through the purifiers with about 5 atm of pressure. Under a typical gas flow rate of about 2 liters/min, it took approximately 2.5 hours to fill the chamber. The entire system was built to whitstand pressures on the order of 10 atm.

After each measurement the xenon from the chamber was recollected to the original stainless steel reservoir kept at liquid nitrogen temperature. With this purification system we have measured that liquid xenon with < 0.3 ppb (oxygen equivalent) is obtained. The purity monitor used for the measurements of the electron lifetime in LXe before capture by impurities is shown in Fig. 10.

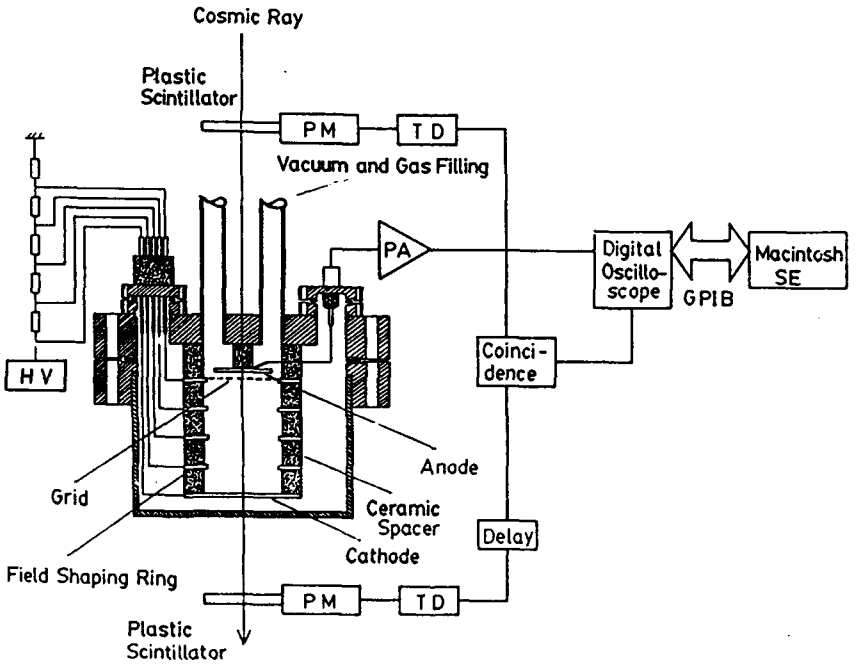

Figure 10. The purity monitor used for the measurements of the electron lifetime in LXe.

From these measurements we have also obtained results on electron drift velocity and low field electron mobility in LXe at the temperature of 195 K, at which the xenon gas was condensed.

These results are very encouraging toward the reliable application of the xenon purification system developed at Columbia to the final goal of a large area/volume detector. Although the problem of purifying xenon from oxygen-like impurities has been solved, further studies will be needed to identify and remove other types of electronegative substances, which can still limit the maximum charge signal in liquid xenon. Results from the work on the purification of LAr and LXe have been published in references 1, 2, 5, and 8.

2.3. Results

2.3.1. *Energy Resolution*

The theoretical energy resolution of a liquid xenon ionization chamber is expected to be similar to that of a Ge(Li) detector from the viewpoint of statistical fluctuations in the total number of charge carriers produced. The two materials have, in fact, a similar WF product where W is the average energy to create an electron-ion pair and F is the Fano factor. The ultimate Fano limited energy resolution $\Delta E/E = 2.35\sqrt{FW/E}$ is based on the assumption that the total number of liberated charges is collected in a liquid ionization chamber. Charge carriers are however lost through electron-ion recombination, attachment to electronegative impurities and trapping by the shielding grid. While the last two effects can be more easily minimized by an effective purification system and by an optimized detector geometry, the effect of electron-ion recombination dominates in high density media and is more difficult to overcome in practical situations. Furthermore, a complete model of the recombination process does not exist, and only more data on its dependence on both electric field and ionization density will allow a more realistic picture of the complex mechanism of electron transport in noble liquids.

In this respect the detailed measurements of the Columbia group carried out within the DARPA funded development represent a major contribution to a better understanding of the basic factors influencing the spectral performance of LAr and LXe detectors. The electric field dependence of the collected charge and the energy resolution of fast electrons, gamma-rays and alpha particles has been systematically measured in LAr and LXe, purified with the systems described above. Figures 11 and 12 show typical energy spectra measured in LAr and LXe with electrons and γ-rays from a ^{207}Bi or ^{241}Am radioactive source. The intrinsic energy resolution of 26 keV (FWHM) for 1 MeV electrons in LAr and of 34 keV (FWHM) for 570 keV γ-rays in LXe is the best reported so far in the literature and is much better than that achievable with NaI(Tℓ). It is however still far from the theoretical prediction based on the Fano factor. To explain this discrepancy we have modified the assumptions of the recombination model generally used to interpret the saturation characteristics of the charge yield as a function of electric field, to include the production of low energy delta-electrons along the primary ionizing particle's track. Statistical fluctuations associated with the high rate of recombination between electrons and ion pairs produced on the heavily ionizing delta-electron tracks, dominate the observed energy resolution much more than fluctuations associated with the Fano factor. This hypothesis, consistent with our data, has provided for the first time a good explanation of the limited energy resolution results in noble liquid detectors. Three publications have been the subject of this work by the Columbia group (Ref. 1, 2, 5).

2.3.3. *Photosensitive Dopants*

The influence of the recombination process on the maximum energy resolution achievable in an ionization device cannot be stopped completely, but increasing the electric field or equivalently increasing the electron mobility would highly reduce its rate. A more practical and effective way to recover the charge lost to recombination is however by doping the pure liquid with photosensitive molecules which have an

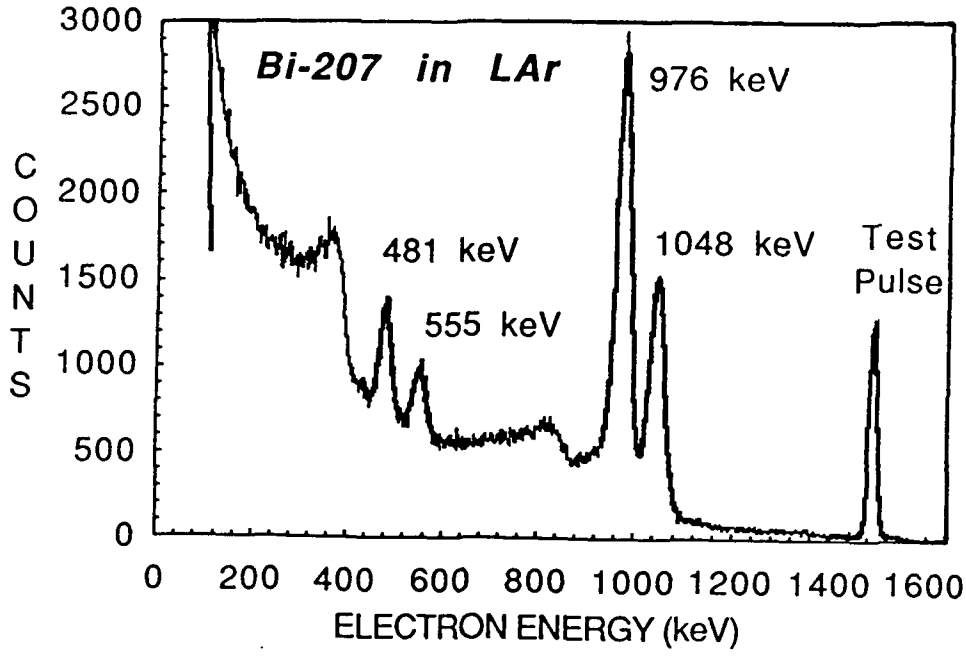

Figure 11. Energy spectrum of ^{207}Bi electrons in liquid argon.

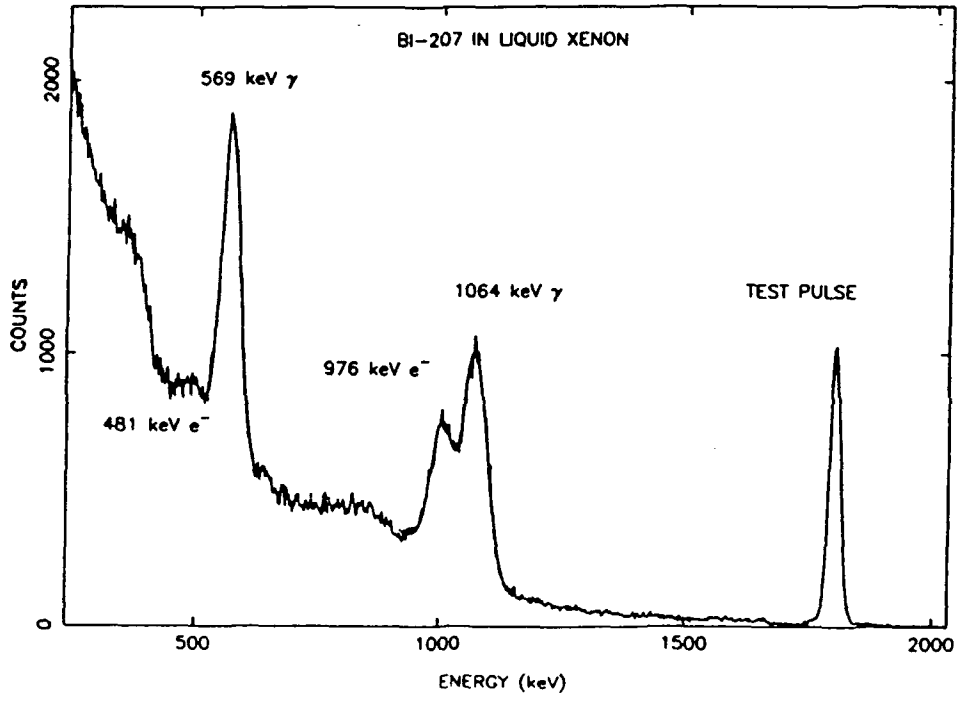

Figure 12. Energy spectrum of ^{207}Bi electrons in liquid xenon.

ionization potential lower than the energies of the UV scintillation photons emitted during the recombination process. These molecules may then be ionized by the photons, producing additional ion pairs. An increase in the number of charges collected and a corresponding improvement in energy resolution is therefore expected. In an attempt to improve the observed resolution in LAr we carried out measurements of α-particles charge yield in argon doped with various concentrations of allene (C_3H_4), one of the most efficient photosensitive dopants investigated so far for LAr. A substantial increase in the amount of charge collected through photoionization was observed, which greatly improved the resolution on the energy of the incident α-particles (Ref. 3).

The effect was less dramatic in the case of fast electrons, due to their much reduced ionizing power with respect to α-particles. The use of non purified dopant presented the further problem of contaminating the pure liquid. We found that even a small amount of non purified allene in a pure liquid argon sample, irradiated with fast electrons, actually decreased the total collected charge because of attachment problems. Measurements with prepurified organic dopants should be part of any future research which aims at improving the energy resolution of LAr and LXe detectors.

2.3.4. *Scintillation Light*

The fast primary scintillation light, abundantly produced in the LXe by an ionizing event is ideal for event triggering. The excellent scintillation efficiency of LXe, comparable to that of NaI(Tℓ), but with shorter decay constants is well established. The UV nature of these scintillation photons ($\sim 170\mu$m) requires the use of exit windows of CaF_2 or BaF_2, coupled with UV sensitive PMT's. The use of wavelength shifters in the LXe volume has to be avoided to preserve the liquid purity. The strong dependence of the scintillation light on the ionization density of the event makes its detection ideal also for background rejection purposes.

In order to detect the light signal produced in LXe by an ionizing particle, we

have designed, built and tested a prototype scintillating chamber equipped with a CaF_2 window sealed with an indium wire to the chamber's body and coupled with a special UV sensitive PMT (Fig. 13).

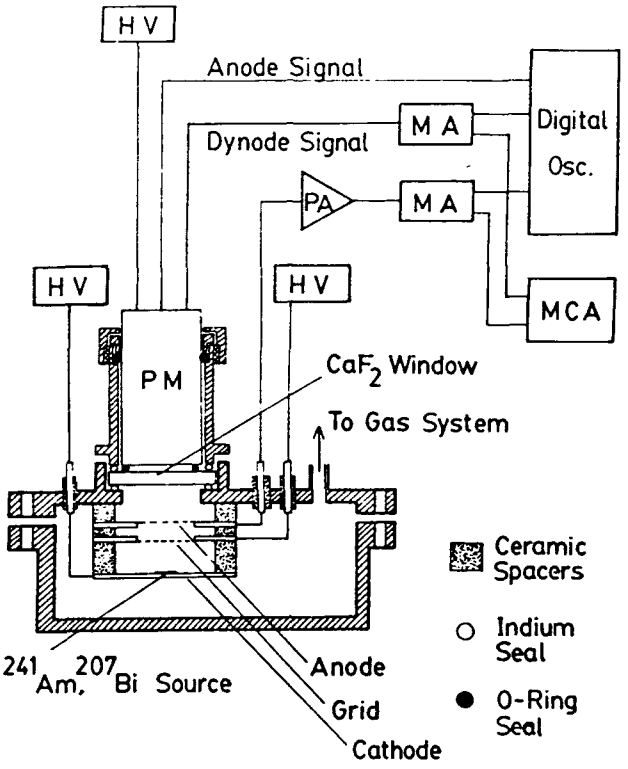

Figure 13. Schematic view of the prototype scintillation chamber and the associated electronics.

We have been successful in operating this chamber at LXe temperature despite the presence of the indium sealed window. The scintillation light pulse from ^{241}Am α-particles and ^{207}Bi electrons, the corresponding charge signal and their correlation was measured. Results shown in Figures 14–16 were published in reference [7].

The design of an optimized ionization/scintillation chamber for imaging studies has been completed and is shown in Fig. 17.

In order to fully demonstrate the imaging capability of a LXe instrument, more R&D efforts are needed given the novelty of the field and its complexity.

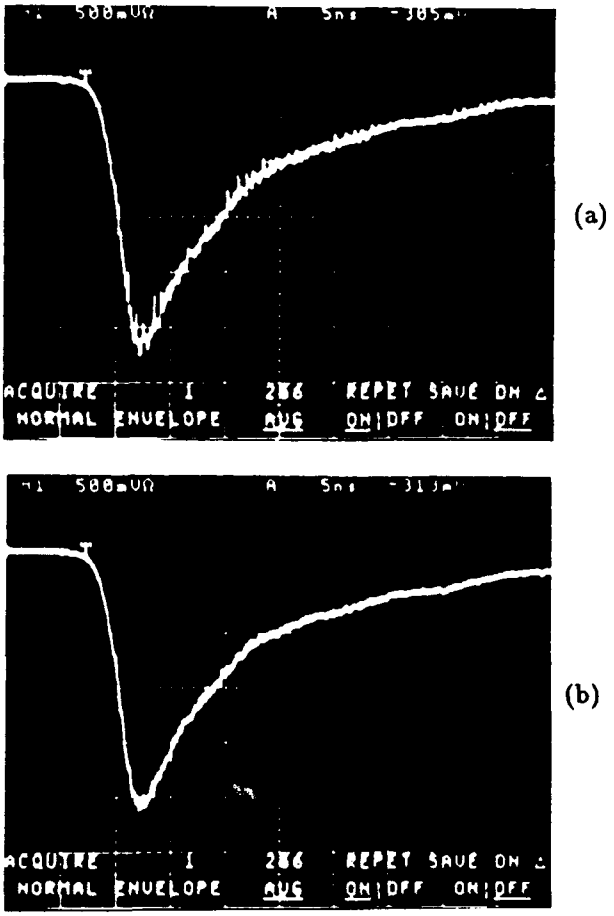

(a)

(b)

Figure 14. Scintillation light of ^{241}Am alpha particles in liquid xenon (a) without and (b) with an applied electric field of 7.9 kV/cm (500 mV/div., 5 nsec/div.).

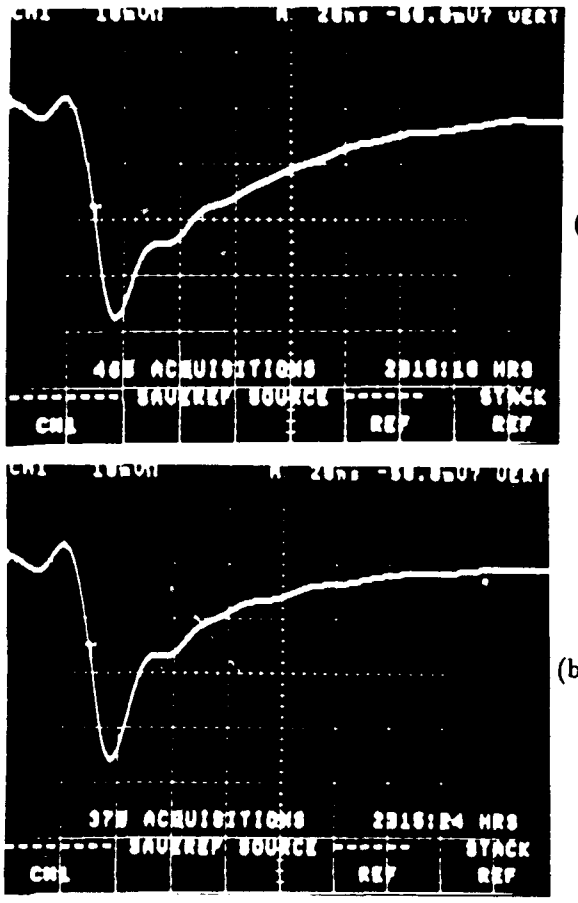

(a)

(b)

Figure 15. Scintillation light of ^{207}Bi conversion electrons in liquid xenon (a) without and (b) with an applied electric field of 2 kV/cm (10 mV/div., 20 nsec/div.).

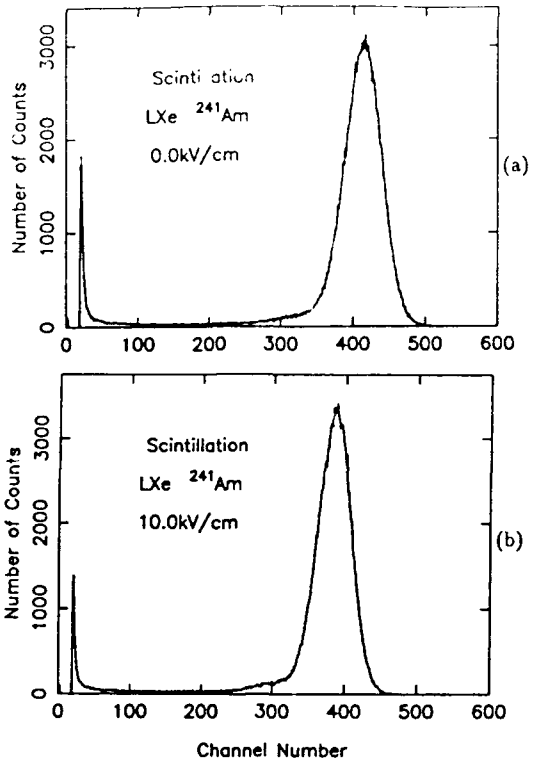

Figure 16. ^{241}Am energy spectrum obtained from the scintillation in liquid xenon (a) without and (b) with an applied electric field of 10 kV/cm.

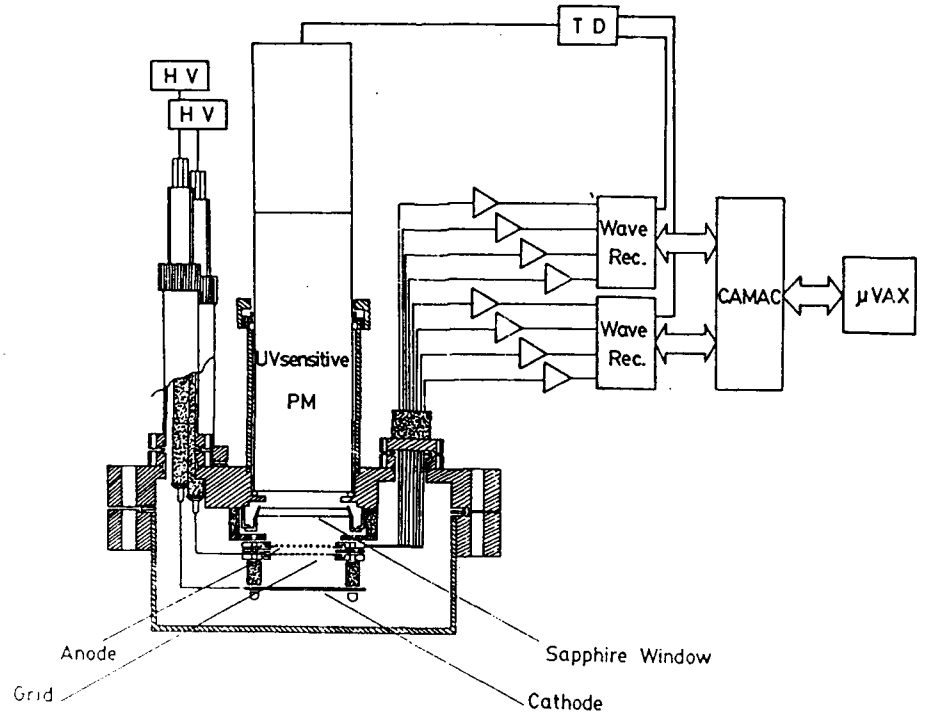

Figure 17. Schematic drawing of optimized ionization/scintillation chamber for imaging studies.

References

[1.] E. Aprile, W. H.-M. Ku, J. Park, and H. Schwartz, "Energy Resolution Studies of Liquid Argon Ionization Detectors," *Nucl. Instr. and Meth.*, **A261**, 519 (1987).

[2.] E. Aprile, W. H.-M. Ku, and J. Park, "Delta Electron Production and the Ultimate Energy Resolution of Liquid Argon Detectors," *IEEE Trans. Nuclear Sci.* Vol. 35, No. 1, 37, (1988).

[3.] E. Aprile, "On the Development of Liquid Ionization Detectors as Spectroscopic Instruments," *Proceedings of the NATO Advanced Study Institute, The Liquid State and its Electrical Properties,* July 1987, Sintra, Portugal. NATO ASI Series B: Physics Vol. 193, p. 540. Edited by E. Kunhardt, L. Christophoru and L. Luessen.

[4.] E. Aprile and M. Suzuki, "Development of a Liquid Xenon Time Projection Chamber for Gamma-Ray Astronomy," *Proceedings of the Workshop on Nuclear Spectroscopy of Astrophysical Sources*, Dec. 14-16, 1987, Washington, D.C. *AIP Conference Proceedings 170*, p. 472. Edited by N. Gehrels and G. Share.

[5.] E. Aprile and M. Suzuki, "Development of Liquid Xenon Detectors for Gamma-Ray Astronomy," in *IEEE Trans. Nucl. Sci*, Vol. 36, No. 1, 311 (1989).

[6.] E. Aprile, R. Mukherjee and M. Suzuki, "A Liquid Xenon Imaging Telescope for 1 – 30 MeV Gamma-Ray Astrophysics," *Proceedings of the SPIE 33rd Annual International Symposium on Optical and Optoelectronics Applied Science and Engineering*, August 6 – 11, 1989, San Diego.

[7.] E. Aprile, R. Mukherjee and M. Suzuki, "A Study of the Scintillation Light Induced in Liquid Xenon by Electrons and Alpha Particles," *Proceedings of the IEEE 1989 Nuclear Science Symposium*, January 15 – 19, 1990, San Francisco.

[8.] E. Aprile, R. Mukherjee and M. Suzuki, "Measurements of the Lifetime of Conduction Electrons in Liquid Xenon," (submitted to *NIM*, June 1990).

ATTACHMENTS

Nuclear Instruments and Methods in Physics Research A261 (1987) 519–526
North-Holland, Amsterdam

ENERGY RESOLUTION STUDIES OF LIQUID ARGON IONIZATION DETECTORS

Elena APRILE, William Hsin-Min KU, Jun PARK and Hugh SCHWARTZ

Department of Physics, Columbia University, New York, New York 10027, USA

Received 3 April 1987 and in revised form 15 June 1987

A gridded ionization chamber was used to study the energy resolution in liquid argon with electrons from a ^{207}Bi radioactive source. Argon was purified in the gas phase with a simple and reliable system, capable of reducing the impurity level below 1 ppb O_2 equivalent, as inferred by a pulse shape analysis of the ionization signals. The electron spectrum was measured at different drift fields, up to 10.9 kV/cm. At this maximum field, a total energy resolution of 32 keV (fwhm), corresponding to a noise-subtracted energy resolution of 26 keV (fwhm), was obtained for the 976 keV conversion electron line. This value is the best reported so far in liquid argon but is still a factor of seven worse than the theoretical limit set by the Fano factor. The reasons for this discrepancy are discussed.

1. Introduction

Liquid rare gases, especially argon and xenon, have properties which make them very interesting media for radiation detectors (table 1). The high atomic number and the high density of liquid xenon (LXe) make it particularly well suited for gamma-ray detection, with an efficiency comparable to that of CsI (Tl). The energy resolution in the ionization mode is theoretically limited by the Fano factor [1], which expresses the degree of statistical fluctuations in the number of electron–ion pairs produced in the liquid by the ionizing radiation. For xenon the calculated Fano factor, $F = 0.041$, and the measured average energy to create an ion pair, $W = 15.6$ eV, give a product $WF = 0.64$, comparable to a product of 0.61 for germanium. The ultimate energy resolution (fwhm) is predicted to be 2 keV for LXe and 4 keV for liquid argon (LAr) at 1 MeV [2]. Among the several measurements in LAr and LXe [3–10] reported in the literature so far, the best experimental energy resolution, both in argon [6] and in xenon [8,10], is still far from the theoretical limits. The factors which contribute most to the degradation of the energy resolution of a gridded ionization detector are: (a) charge loss mechanisms such as recombination between electrons and positive ions, attachment of free electrons to electronegative impurities, and electron trapping by the grid; (b) electronic noise. Backscattering in the source material, variation of pulses rise time, and imperfect grid shielding will add much smaller terms to the measured energy resolution.

Table 1
Properties of argon and xenon

Property	Argon	Xenon	Unit
Atomic number	18	54	
Atomic weight	39.95	131.3	g/mol
Boiling point	−185.9	−109.1	°C
Melting point	−189.4	−111.8	°C
Density (1 bar, 15 °C)	1.6689	5.517	kg/m^3
$T_{critical}$	−122.43	16.59	°C
$P_{critical}$	48.65	58.40	bar
Properties of liquids			
Volume ratio	784.0	518.9	(gas/liquid)
Vap. enthalpy	163.4	99.3	J/g
Density	1.4	3.06	g/cm^3
v_d at 1 kV/cm	2.2	2.4	mm/μs
Mobility	525	2000	cm^2 V^{-1} s^{-1}
Radiation length	13.5	2.6	cm
W-value	23.6	15.6	eV/pair
$(dE/dx)_{min}$	2.2	3.9	MeV/cm
Fano-factor	0.11	0.041	
WF	2.54	0.64	eV

In order to understand the influence of these limiting factors on the energy resolution achievable with liquid detectors, we have built a gridded ionization chamber to be used for energy resolution measurements with electrons and alpha particles in both LAr and LXe. In this paper we present the results obtained so far in LAr with the electron source.

2. Detector system design

2.1. Detector

A schematic view of the detector is shown in fig. 1. It is a gridded ionization chamber with two parallel plates,

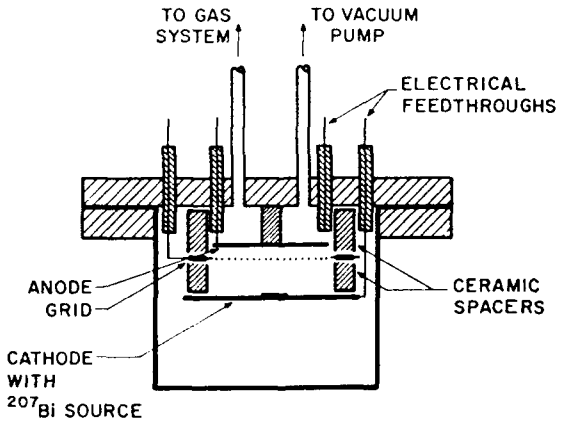

Fig. 1. Schematic cross section of the gridded ionization chamber.

the anode and the cathode, separated by a grid. The grid is essential to obtain a position-independent ionization signal Since the mobility of the positive ions is several orders of magnitude lower than that of the electrons, only the drifting electrons contribute to the observed signal. The cathode and anode of the chamber are circular stainless steel disks of 6 cm and 4 cm diameter, respectively. The grid is made out of 50-μm thick electroformed nickel mesh with 99-μm wide lines spaced 846-μm apart, bonded on a nickel ring [11]. The anode–grid and cathode–grid separation could be easily varied by using ceramic spacers of different thickness. The data presented in this paper were obtained with a 2.9-mm spacing between anode and grid and a 6.2-mm spacing between grid and cathode. With this geometry the shielding inefficiency of the grid, calculated according to Bunemann [12], is 4.7%. The transparency to drifting electrons is calculated to be 100% when the collection field (between anode and grid) is at least 2.1 times stronger than the drift field (between grid and cathode). We note however that Bunemann's formulae apply to grids made of single wires of circular cross section, and are therefore only approximate in the case of meshes.

The assembled electrode structure is contained in a stainless steel vessel of 75-mm internal diameter and 350-cm^3 total volume. The vessel is sealed with a copper gasket to a stainless steel top flange, from which the structure is suspended. The gas supply lines and the electrical feedthroughs are welded on this top flange.

2.2. Gas handling and purification

A schematic drawing of the gas purification system with the rest of the support system is shown in fig. 2. The system is built with ultrahigh vacuum techniques, using only clean and bakeable materials. The stainless steel tubing of the gas system are either welded or connected with high vacuum fittings, and only metal bellow valves are used [13]. Before assembly, each part of the whole system was carefully cleaned and the closed system was kept under vacuum for several days. The vacuum at the ion pump was better than 10^{-8} Torr and the detector outgassing rate less than 10^{-8} Torr l/s. The purification system uses a combination of active and passive materials. Commercial grade argon gas is first passed through an Oxisorb purifier [14], which removes most of the oxygen by chemisorption on a highly active metallic surface supported on an inert base, and some of the water by adsorption on molecular sieve. After this first stage, the gas flows through two molecular sieves of the type 13X and 4A [15], contained in two separate 1.8 liter stainless steel vessels. The sieves were operated at dry ice temperature, for better adsorption efficiency. This simple sequence is capable of purifying argon gas to a level below 1 ppb of O_2 equivalent, as demonstrated by Aprile et al. [16]. The molecular

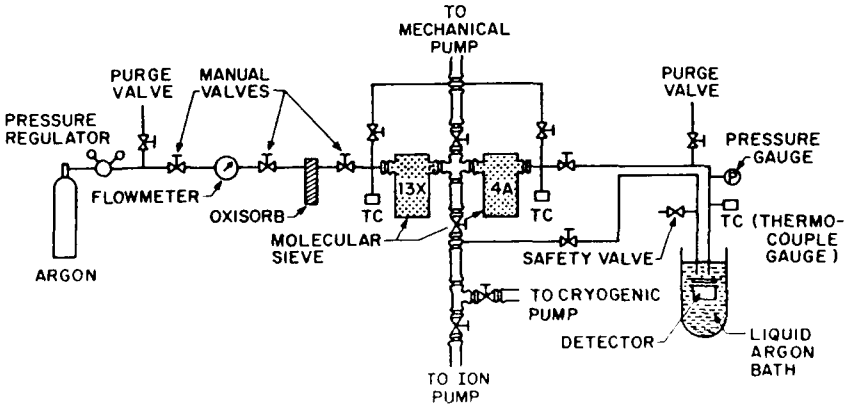

Fig. 2. Schematic drawing of the gas handling and purification system.

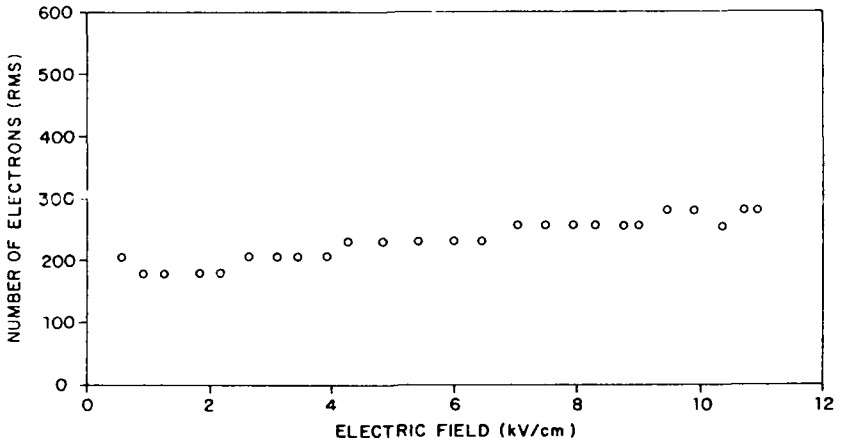

Fig. 3. The equivalent noise charge (rms) as a function of the drift field.

sieves were initially baked out to 200 °C under vacuum for several days. Generally, the vacuum and counter performance improved dramatically for the first two days, and gradually thereafter. Extended pumping beyond a week produced little improvement. The sieves were always baked out under vacuum in between runs.

The purified argon gas was condensed in the detector and maintained in the liquid state by surrounding the sealed vessel with a LAr bath in an open cryostat. The chamber requires 274 l atm of argon gas. It was filled with argon flowing through the Oxisorb and sieves at a rate of about 3.5 l/min. Slower rates were tried but did not yield improved performance.

2.3. Electronics

The charge signal collected on the anode was processed by a low-noise charge-sensitive preamplifier. To avoid the additional capacitance of long signal cables the input FET and the feedback network were mounted directly on top of the chamber, in a sealed box cooled by the LAr bath. The equivalent noise charge of the preamplifier was measured to be ~ 160 electrons (rms) at room temperature with a detector capacitance of 17 pF. With the cooling bath around the chamber, the noise level increased slightly, despite the cooled FET, mostly because of microphonic noise associated with the bubbling LAr in the open dewar. The signal from the preamplifier was fed to an Ortec-450 shaping amplifier and digitized by an ND-65 multichannel analyzer.

The negative high voltage to the cathode and to the grid was respectively supplied by a Spellman (0–20 kV) and a Power Design (0–6 kV) unit, both with ~ 0.001% ripple. For the higher drift field data a 10 kV Bertan unit was used for the grid. A resistive-capacitive network, encapsulated in epoxy, provided additional filtering for the power supplies. The noise level generally increased with the HV applied to the chamber. Fig. 3 shows the dependence of the equivalent noise charge (rms) on the drift field strength, during a typical run. The best noise resolution was obtained with bipolar shaping and 5-μs differential and integral time constants.

Table 2
Radiation from ^{207}Bi

Energy [keV]	Transition	Relative intensity	
10.8	Pb L_{III}–M_V	50	
13.0	Pb L_{II}–M_{IV}	25	
72.8	Pb K–L_{II}	1800	
75.0	Pb K–L_{III}	3700	
84.9	Pb K–M_{II-III}	1460	
87.3	Pb K–N_{II-III}	155	
553.8	Pb L_I conv	18	
554.4	Pb L_{II} conv	20	
556.6	Pb L_{III} conv	5	
566.0	Pb M conv	15	
569.6	Pb γ	9775	Compton edge: 408
897.7	Pb γ	12	
975.6	Pb K conv	719	
1047.8	Pb $L_I$conv	132	
1048.4	Pb L_{II}conv	35	
1050.6	Pb L_{III}conv	11	
1060.0	Pb M conv	59	
1063.6	Pb γ	7408	Compton edge: 858
1442.2	Pb γ	13	
1682.2	Pb K conv	2	
1770.2	Pb γ	701	Compton edge: 1546 Escape peaks: 1259 748

The calibration of the whole readout chain was made with a test pulse coupled with a 1 pF capacitor to the gate of the FET. The overall systematic uncertainty on the charge measurement is estimated to be ~ 7%.

For a measurement of the LAr purity, pulse shape analysis of the ionization signals was performed using a Tektronix 2430 digital oscilloscope. For these tests single ionization pulses from the charge sensitive preamplifier were recorded, with the decay time constant of the input stage set to 1 ms to enable the observation of very long drift times.

2.4. Radioactive source

0.1 μCi (7400 disintegrations/s) of $^{207}_{83}$Bi was electropolated on a 5-mm diameter spot in the center of the cathode disk. $^{207}_{83}$Bi is a β^+-decay radioactive source. The principal lines from the 30-yr half-life source are 2 nuclear γ-ray lines at $E_\gamma = 569.6$, and 1063.6 keV plus a weaker line at 1770.2 keV. However in a shallow argon counter, the measured pulse height peaks are mostly due to internal conversion electrons at $E_\gamma - K_{ab} = 481.6$ and 975.6 keV, and $E_\gamma - L_{ab} = 554.4$ and 1047.8 keV, where $K_{ab} = 88.0$ keV and $L_{ab} = 15.9$, 15.2, and 13.0 keV are the K-edge and L-edge energies of $^{207}_{81}$Pb. MeV electrons have a range of about 3 mm in argon and are therefore completely adsorbed in the active detector volume, whereas the γ-rays are not fully absorbed. Pb K-fluorescence photons and Auger electrons at ~ 74.3 [K_α] and ~ 86.4 keV [K_β] are also emitted, and, in fact, dominate the low energy spectrum. Table 2 gives a summary of the major transitions and their relative strengths expected from ^{207}Bi.

3. Results

3.1. Measurement of the LAr purity

Electronegative impurities limit the energy resolution of a liquid ionization detector because the drifting electrons will easily attach to such substances, with a consequent reduction of the total collected charge. The attenuation length, λ (cm), defined as the distance in which the total charge decreases by a factor of e, is proportional to the drift field E (kV/cm) and inversely proportional to the impurity concentration ρ (ppm O_2 equivalent):

$$\lambda = \alpha E/\rho, \qquad (1)$$

where the trapping constant α has a value of 0.15 cm^2 ppm kV^{-1} for LAr [11].

To measure the attenuation length is equivalent to measure the attenuation time $\tau = \lambda/v_d$, where v_d is the electron drift velocity. For typical 1 kV/cm drift fields one would need unpractically long chambers. Alternatively, one can reduce the applied field and thus increase the drift time of the electrons. A measurement of the maximum drift time would then yield directly the impurity concentration. For these tests cosmic ray particles traversing the whole chamber were used as ionizing radiation. The drift region was set to 30 mm and the anode–grid distance was set to 4.2 mm.

The charge signal from a uniform track of ionization in a gridded chamber filled with a pure liquid rises linearly with time until all electrons reach the anode. If electron trapping impurities are present the pulse shape is modified and can be expressed by

$$Q(t) = Ne(\tau/t_d)(1 - e^{-t/\tau}), \qquad 0 \leqslant t \leqslant t_d, \qquad (2)$$

where Ne is the total charge left in the drift region after recombination, t_d is the drift time, and τ is the attenuation time. Eq. (2) is an approximation valid in the case

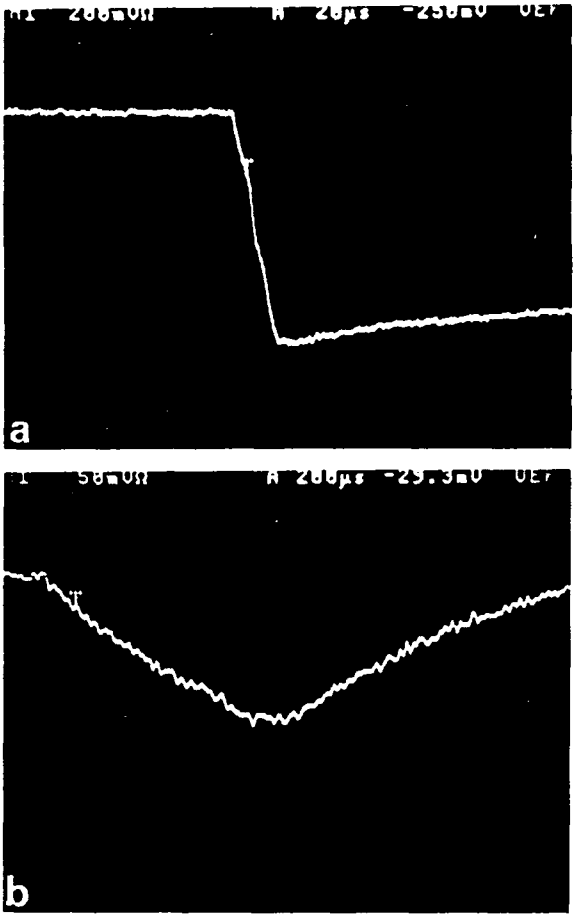

Fig. 4. Digital oscilloscope pictures of ionization pulses in LAr from cosmic rays traversing the chamber: (a) Single pulse at a drift field of 900 V/cm. The horizontal scale is 20 μs/div. (b) Single pulse at a drift field of 10 V/cm. The horizontal scale is 200 μs/div.

the electrons drift time between the cathode and the grid is much longer than that between the grid and the anode.

By using a waveform digitizer, the shape of the signals was recorded and analyzed. The drift field was lowered below 10 V/cm and the longest observed drift time was ~ 800 μs. Fig. 4 shows typical pulses at 900 V/cm and 10 V/cm. The observed electron lifetime corresponds to an impurity concentration of < 1 ppb (oxygen equivalent).

3.2. Measured pulse height spectra

Fig. 5a shows the $^{207}_{83}$Bi pulse height spectrum measured with our LAr chamber. The drift field was 10.9 kV/cm and the collection field was three times as large for maximum grid transmission (see fig. 6). A test pulse is shown to the right. Its width indicates a noise contribution of 18.5 ± 0.8 keV (fwhm). The dominant 975.6 keV electron peak is visible with an energy resolution of 31.9 ± 1.4 keV (fwhm) – well resolved from the 1048 keV peak. Two smaller peaks corresponding to the 481.6 and 554.4 keV electrons are also observed. Additional broad features corresponding to the 408 and 858 keV Compton edges can also be identified. The statistics is good enough to suggest that the dominant L transition for the 1064 and 570 keV γ-ray is L_I and L_{II}, respectively. The heavy solid line in fig. 5a incorporates 6 Gaussians, two linearly varying baseline segments plus an exponential noise function to fit the 4 nuclear lines plus the two atomic lines. An intrinsic resolution of 26.0 ± 1.6 keV (fwhm) at 976 keV, scaled as $E^{1/2}$ to other energies, plus the 18.5 keV electronic noise (fwhm), was found to model the data adequately. Fig. 5b is a log–linear plot of the electron spectrum recorded at the same electric field over 20 min in order to detect the 1682 keV K-conversion electrons associated with the weak 1770 keV γ-ray line. The Pb K-fluorescence photons are also clearly visible in the low energy end of the spectrum. The test pulse was removed for this run.

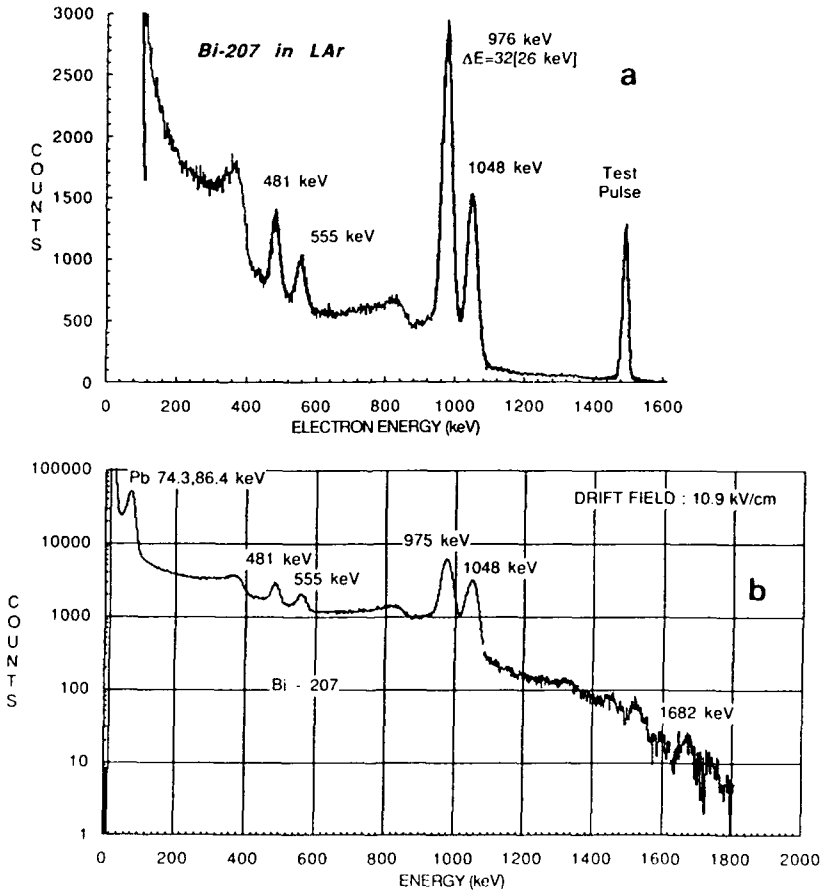

Fig. 5. Pulse height spectrum of the ^{207}Bi radioactive source in LAr. The drift field is 10.9 kV/cm. The 976 keV electron peak is visible with a total energy resolution of 32 keV (fwhm). A test pulse with 18.5 keV (fwhm) of electronic noise is shown to the right. The heavy solid line is the best Gaussian fit to the data. (a) Counts versus electron energy; (b) log counts versus electron energy for the same spectrum accumulated over 20 min.

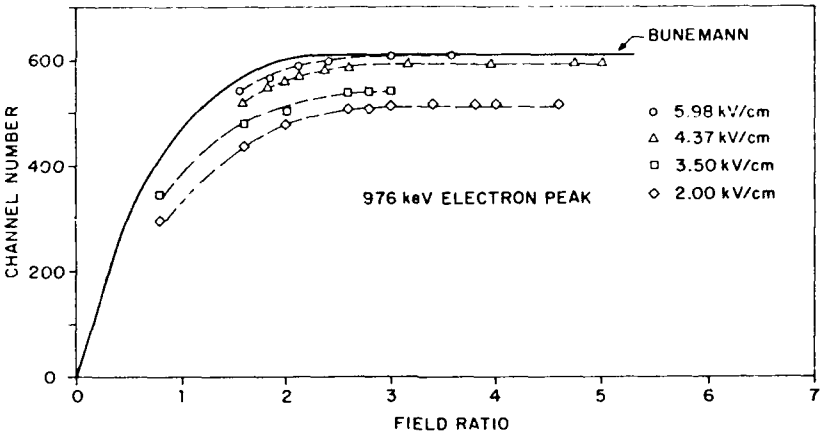

Fig. 6. Pulse height of the 976 keV electron peak as a function of the ratio of collection field to drift field, at four different drift field strengths. The solid line is the Bunemann prediction normalized at 6 kV/cm.

3.3. Pulse height performance

The pulse height performance of the counter was first checked at different values of the ratio $E_{\text{collection}}/E_{\text{drift}}$ in order to optimize the grid transmission. Fig. 6 shows the pulse height of the 976 keV electron peak at four drift field values, from 2 to 6 kV/cm, as a function of the field ratio. The solid line is Bunemann's prediction normalized for the charge collected at 6 kV/cm [12]. The measurements indicate that at least a ratio of 3 is necessary for maximum charge collection up to a field of ~ 6 kV/cm. In fig. 7 we show the dependence of the collected charge, for the 976 keV electron peak, on the drift field. The solid line is a fit to the data, including the low field points, with the function $Q/Q_0 = (1 + K/E)^{-1}$ based on the Jaffe theory for columnar recombination [18,19]. In this expression Q is the collected charge, Q_0 is the charge extrapolated to infinite electric field E, and K is the recombination coefficient. The best fit values are $Q_0 = 6.35 \pm 0.5$ fC and $K = 0.274 \pm 0.06$ kV/cm, where the error on Q_0 is dominated by the systematic error on the charge

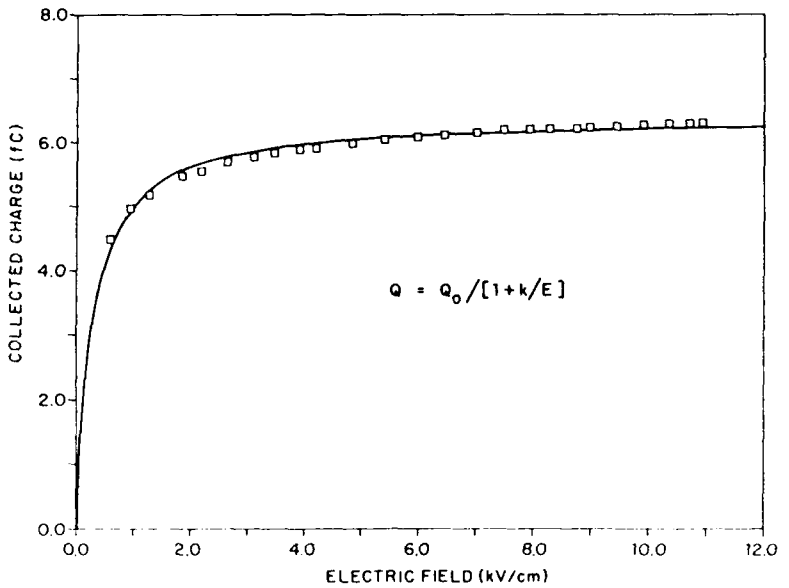

Fig. 7. Collected charge (in fC) for the 976 keV electrons as function of drift field. The solid line is a fit to the data, based on columnar recombination theory.

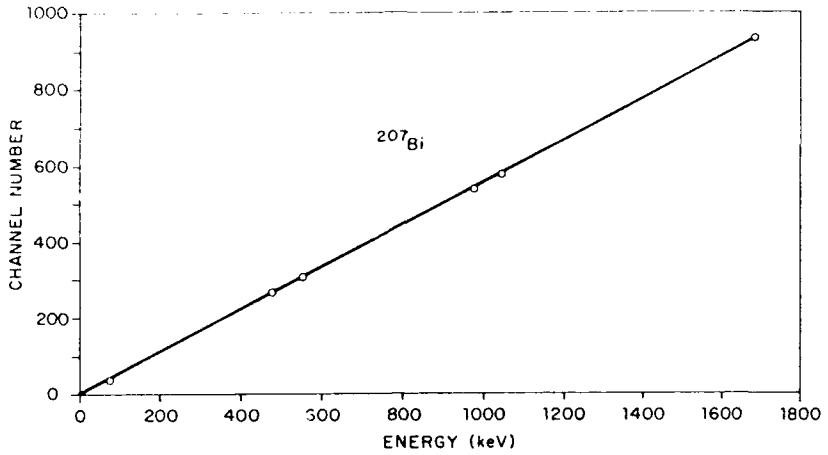

Fig. 8. The pulse height proportionality of the chamber: peak channel of the five electron lines and the two fluorescence photon lines versus nominal energy. The solid line is a straight line fit to the data.

calibration. Assuming 23.6 eV as average energy to produce an electron–ion pair in LAr, the total charge released by a 976 keV electron is 6.6 fC implying (96 ± 7)% collection efficiency.

Fig. 8 checks the pulse height proportionality of the detector. The peak channel corresponding to each feature in the measured spectrum (fig. 5) is plotted against the nominal energy. A straight line fits the data fairly well.

The pulse height stability was checked each time measurements were made with one argon filling, by recording the spectrum for the same detector conditions at the beginning and the end of the run. Less than 0.5% gain change was observed over a maximum period of 30 h, indicating a very clean chamber with low residual outgassing rate.

4. Discussion

The total fwhm energy resolution as a function of the incident energy E, is given by:

$$\Delta E = 2.35\left[FWE + \sigma_e^2 + \sigma_t^2 + \sigma_r^2 \right]^{1/2}, \qquad (3)$$

where $F = 0.11$ is the Fano factor for LAr, $W = 0.024$ keV is the mean energy to create an ion pair, $\sigma_e \sim 8$ keV is the electronic noise contribution, $\sigma_s \sim \eta(s/q)E \sim 3.5$ keV is the estimated contribution due to imperfect shielding by the grid and depends on the range of the incident electrons ($\eta = 0.047$ is the shielding inefficiency, $s = 0.7$ mm is the standard deviation of the projected track length distribution for 976 keV electrons and $d = 9.1$ mm is the anode–cathode distance), σ_t caused by the thickness of the source is on the order of a few electron volts and σ_r is caused by the variation in pulse rise time, due to different track orientations. Amplifier shaping constants longer than pulse collection times minimize this last effect. Clearly the first two terms in eq. (3) dominate the measured spread in energy resolution, especially since we expect the shielding inefficiency of the mesh to be lower than the calculated 4.7%. To estimate the intrinsic energy resolution of the detector we therefore subtract only the variance term caused by the well-defined electronic noise.

To determine which electron loss process contributes most to the energy resolution, we examined the energy resolution as a function of the drift field, at a fixed field ratio of 3. Maintaining the field ratio constant keeps the grid losses constant and allows us to examine just the effects of varying electron attachment and recombination. At high drift fields, the latter should dominate. Fig. 9 displays the intrinsic energy resolution (fwhm) of the 967 keV electron line against the electric field strength. The data points are from three different measurements. The consistency of the results, within errors, is apparent. The resolution degrades much faster with collected charge than the inverse law expected for the case where the fluctuations are proportional to the total charge generated. It is hard to explain the observed dependence in terms of nonsaturation effects of the collected charge, since from the saturation curve (fig. 7) it appears that at the highest applied field about (96 ± 7)% of the total generated electrons are collected. At present the recombination phenomenon is not fully understood and more precise measurements, together with a more realistic model, are needed to explain the physical processes responsible for the observations.

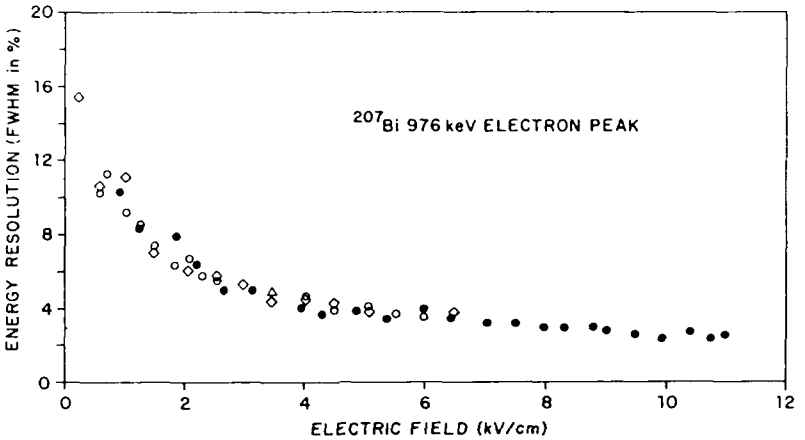

Fig. 9. Noise-subtracted energy resolution (fwhm) of the 976 keV electron line as a function of the drift field. The data points are from three different runs.

5. Conclusion

The energy resolution response of a LAr ionization chamber was tested with electrons from a ^{207} Bi radioactive source. The spectrum, dominated by several conversion electron lines, was measured at different field strengths, up to 10.9 kV/cm. At this highest field, a total resolution of 32 keV (fwhm) was obtained for the dominant 976 keV electron line. The noise-subtracted value of 26 keV (fwhm) is still a factor of 2 worse than the Poisson statistical limit and a factor of 7 worse than the Fano limit, but it is the best reported so far in LAr.

A simple and reliable purification system was used to obtain LAr with less than 1 ppb (O_2 equivalent) impurity concentration, as inferred by a pulse shape analysis of the ionization pulses. Consequently, electron attachment to electronegative substances is not a major problem in our detector. Electron trapping by the grid should also be negligible, since we have directly measured the collection to drift field ratio necessary for maximum grid transmission efficiency. Fluctuations in the magnitude of the total ionization signal, associated with recombination processes on the primary-electron track and mostly on delta-electron tracks, are therefore believed to dominate the measured energy resolution. A better understanding of this mechanism is needed in order to overcome its limitations. Increasing the electric field or alternatively, increasing the electron mobility at a moderate field, would reduce the rate of recombination and thus improve the energy resolution. Finally, better electronic noise resolution and, to less extent, better grid parameters are necessary. In this respect we plan to continue investigating with liquid ionization detectors to reach their best energy resolution performance. A variety of interesting applications are already possible even with a detector resolution close to the Poisson limit.

Acknowledgements

We wish to thank Robert Novick for helpful discussions and guidance. We acknowledge Erich Jauch and Irwin Rochwarger for their valuable engineering support. This research was supported by a grant from DARPA-ONR under contract number N00014-86-K0494.

References

[1] U. Fano, Phys. Rev. 72 (1947) 29.
[2] T. Doke, A. Hitachi, S. Kubota, A. Nakamoto and T. Takahashi, Nucl. Instr. and Meth. 134 (1976) 353.
[3] J.H. Marshall, Phys. Rev. (1953) 905.
[4] J.H. Marshall, Rev. Sci. Instr. 25 (1954) 232.
[5] E. Shibamura, A. Hitachi, T. Doke, T. Takahashi, S. Kubota and M. Miyajima, Nucl. Instr. and Meth. 131 (1975) 249.
[6] M.D. Edmiston and C.R. Gruhn, IEEE Trans. Nucl. Sci. NS-25 (1978) 352.
[7] Th. Lindblad, L. Bagge, A. Engstromand and J. Bialkowski, Nucl. Instr. and Meth. 251 (1983) 183.
[8] K. Masuda, A. Hitachi, Y. Roshi, T. Doke, A. Nakamoto, E. Shibamura and T. Takahashi, Nucl. Instr. and Meth. 174 (1980) 439.
[9] T. Doke, Nucl. Instr. and Meth. 196 (1982) 87.
[10] I.M. Obodovsky and S.. Pokachalor, Low Temp. Phys. 5 (1979) 829.
[11] Buckbee-Mears Company, Saint Paul, Minnesota, USA.
[12] O. Bunemann, T.E. Cranshaw and J.A. Harvey, Can. J. Res. 27 (1949) 191.
[13] Cajon Company, VCR vacuum fittings.
[14] Messer Griesheim GmbH, Oxisorb Gas Purifier.
[15] Union Carbide Corp., Linde Molecular Sieves.
[16] E. Aprile, K.L. Giboni and C. Rubbia, Nucl. Instr. and Meth. A241 (1985) 62.
[17] W. Hofmann, U. Klein, M. Schulz, J. Spengler and D. Wegener, Nucl. Instr. and Meth. 135 (1976) 151.
[18] G. Jaffe, Ann. Phys. 42 (1912) 303.
[19] H.A. Kramers, Physica 18 (1952) 665.

DELTA ELECTRON PRODUCTION AND THE ULTIMATE ENERGY RESOLUTION OF LIQUID ARGON IONIZATION DETECTORS

Elena Aprile, William H.-M. Ku†, and Jun Park
Columbia Astrophysics Laboratory
Columbia University
538 West 120th Street
New York, New York 10027

Abstract

The calculated Fano factor limits the energy resolution in liquid argon ionization chambers to 4 keV (FWHM) at 1 MeV. This theoretical value is several times better than any experimental result reported so far in the literature. We have recently measured an intrinsic energy resolution of 26 ± 2 keV for the 976 keV conversion electrons of a ^{207}Bi source in a gridded ionization chamber filled with pure liquid argon, at a drift field of 11 kV cm^{-1}. The measurement of the ^{207}Bi spectrum at different electric fields was repeated several times, with very good liquid purity and optimized chamber geometry, reproducing the results. Data were also taken with a xenon-doped liquid argon filling in an attempt to improve the resolution. Enhanced ionization was observed as expected from the presence of excitons in liquid argon, but no improvement in the energy resolution. In this paper we show that the data are consistent with the assumption that recombination straggling from low energy delta electrons, produced abundantly along the path of the primary ionizing particle, is mostly responsible for the degraded experimental resolution.

1. Introduction

There has been continuing interest in rare gas liquids and solids for radiation detection in both high energy and nuclear physics, as well as in astrophysics. The high density, small Fano factors, small diffusion constants, and good scintillation properties are some of the characteristics which make these materials ideal for different detector types.

For gamma-ray astronomy the development of a high resolution liquid xenon imaging spectrometer is of primary interest. Such a detector, operated either in the ionization or the proportional scintillation mode, could offer a combination of high spectral and spatial resolutions with large effective areas. Orders of magnitude better sensitivity could be achieved compared to more commonly used germanium or sodium iodide detectors, in an energy range from several keV to several MeV.

Another example of the physics potential of a large volume liquid xenon imaging chamber is the investigation of the double beta decay of ^{136}Xe. We are considering the feasibility of such an experiment. The significantly improved sensitivity with respect to other existing or planned experiments would have great impact on this fundamental research.

For most applications the excellent spectral response predicted for liquid argon and xenon is the most attracting feature of these materials. A calculation of the Fano factor limited resolution [1] predicts about 4 keV and 2 keV (FWHM) at 1 MeV, for liquid argon and xenon respectively. These values are comparable to the ones of solid state detectors.

Confronted with these expectations, the best experimental results reported so far in both liquids seem rather poor [2 - 6]. The discrepancy between theory and experiment is even larger in xenon than in argon, while one would expect the contrary.

The factors which contribute to the energy resolution of an ionization detector include: fluctuations in the number of electron-ion pairs created by the ionizing particle, attachment of free electrons to electronegative impurities, chamber design and electronic noise. The reasons for the degraded resolution have been generally attributed to intrinsic limitations of the experimental apparatus. In particular, the purity of the liquid has been frequently suspected to be insufficient. However, it is difficult to explain the consistency of the results, within experimental errors, obtained with completely different systems. A common physical process could be limiting the observed resolution, much more than any instrumentation related factor.

From measurements with compressed xenon gas, Bolotnikov *et al.* [7] have recently shown that, for xenon densities larger than 0.6 g cm^{-3} the experimental energy resolution is mostly determined by recombination of electron-ion pairs from low energy delta electrons, produced along the primary track. Since the dynamical behavior of free electrons in high pressure rare gases should resemble that in the corresponding liquids we have checked the influence of delta electron production in our liquid argon data. The measurements with fast electrons were repeated with an improved chamber geometry, but results consistent with previously published ones [6] were obtained.

The electric field dependence of the collected charge was analyzed assuming a different recombination rate for the part of the signal produced by delta electrons which have a high ionization density. By taking into account this process a considerably degraded energy resolution is expected than if only ionization straggling described by the Fano factor is taken into account. The predictions are in good agreement with our experimental data. Results obtained in liquid argon with a small concentration of xenon are also discussed.

2. Experimental Method

The experimental system used for the liquid argon tests has been described in detail elsewhere [6]. Here we shall briefly discuss the relevant features and the changes made to improve its performance.

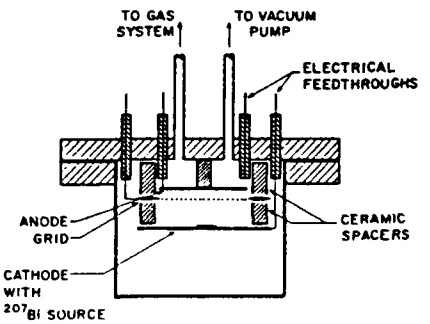

Fig. 1. Schematic View of the Ionization Chamber.

0018-9499/88/0200-0037$01.00 © 1988 IEEE

The ionization chamber, shown schematically in Fig. 1, consists of two circular stainless steel electrodes separated by a grid, made of electroformed nickel mesh on a nickel support ring. The data presented in this paper were taken with a grid having higher shielding efficiency than the previous one, namely 99% for the same grid-anode separation of 2.9 mm.

The drift region was 6.1 mm. A collection field at least three times stronger than the drift field was measured to give maximum transmission for the drifting electrons. The improved grid geometry, however, did not have a significant effect on the energy resolution.

A careful choice of clean materials and an efficient purification system are required to minimize the capture of free ionization electrons by electronegative impurities. In our system argon gas is purified by passing it through an Oxisorb purifier followed by two molecular sieves at dry ice temperature. We have demonstrated in earlier studies [6, 8] that this simple method is capable of reducing the impurity concentration below 1 ppb, equivalent oxygen. The purified gas is condensed into the chamber by surrounding it with a bath of commercial grade liquid argon in an open dewar.

The purification system was modified for tests with xenon-doped argon. The 13X sieve had to be removed since the adsorption of xenon in this zeolite is substantial (in the order of 60 grams per 100 grams of zeolite at -78 °C and 1 atm) [9]. A (Zr-V-Fe) getter [10], operated at 450 °C was added. The 4A molecular sieve, having pores too small to trap xenon, was left in the system. The new system was carefully cleaned before assembly and evacuated to a pressure of about 10^{-7} Torr with a turbomolecular pump. Measurements with liquid argon purified by either purification system are consistent.

As with previous measurements a ^{207}Bi source, electroplated on the cathode, was used to ionize the liquid. Negative high voltage was supplied separately to the cathode and to the grid. The anode was directly coupled to the input stage of a low noise charge sensitive preamplifier. The charge signals were passed through a spectroscopy amplifier and fed into a multichannel analyzer. Bipolar shaping with 3 μs time constants was typically used. At high drift fields, however, a better signal/noise ratio was achieved with 1.5 μs shaping. An average equivalent noise charge of 250 electrons RMS was characteristic of our readout system. A test pulse coupled with a 1 pF capacitor to the gate of the FET served for charge calibration.

3. Results and Discussion

In the shallow liquid argon chamber used for these tests the gamma-ray activity of the ^{207}Bi source is poorly detectable and the spectrum is dominated by four internal conversion electron lines at 481, 555, 976 and 1048 keV. The Compton edges associated with the two gamma-ray lines at 569 and 1064 keV are visible as well as the fluorescence X-rays at the low energy end of the spectrum. A typical pulse height spectrum measured at the highest drift field in our liquid argon chamber is shown in Fig. 2.

We have measured the pulse height spectrum at many different drift field settings from few hundred V cm^{-1} up to a maximum of about 11 kV cm^{-1}. At higher fields repeated breakdown occurred, mostly due to failure of the electrical feedthroughs. Several data sets were taken under similar conditions to cross check the reproducibility of the results. Each spectrum was accumulated for at least 4 minutes, to ensure good statistics, and saved for further analysis. The peak location and the width of the dominant lines were determined by a least squares fit with gaussian functions. The background was approximated by a quadratic function. The resolution was defined as the ratio of the full width at half maximum to the maximum pulse height of the line. The contribution of the electronic noise was determined from the width of the test pulse distribution.

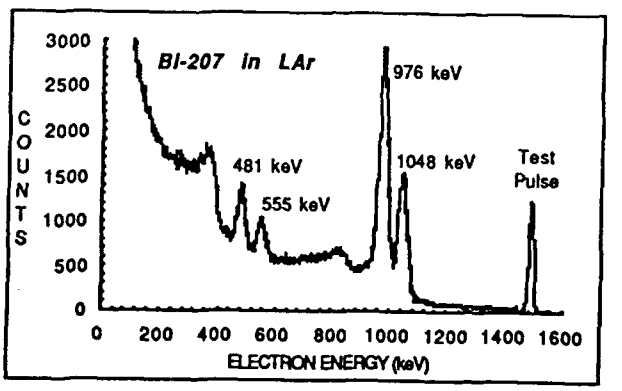

Fig. 2. ^{207}Bi Pulse Height Spectrum in Liquid Argon. The drift field strength is ~ 11 kV cm^{-1}. The energy resolution of the 976 keV electron line is 32 keV (FWHM). The electronic noise contribution is 18.5 keV (FWHM).

3.1. Collected Charge

To interpret the measured electric field dependence of the collected charge we can use the formula based on the Jaffe theory of columnar recombination [11, 12]:

$$Q/Q_0 = 1/(1+k/E), \qquad (1)$$

where Q is the collected charge, Q_0 is the total charge produced along the track of the ionizing particle, E is the electric field and k is the recombination constant. At infinite field no recombination takes place and Q equals Q_0. The total number of electron-ion pairs produced by a 976 keV electron in liquid argon is ~ 4 x 10^4 or 6.6 fC, assuming an average energy (W) to create one pair of 23.6 eV.

A fit to our data with Eq. (1) gives Q_0 = 6.21 ± 0.03 fC and k = 0.28 ± 0.01 kV cm^{-1} with a χ^2 of 18 per degree of freedom. The errors are statistical only. A systematic uncertainty of about 5% from the charge calibration should be added to the absolute determination of the measured charge. Analyzed in this way the data are consistent with a fraction of charge escaping recombination close to 100% making it impossible to explain the measured values for resolution.

The track of the fast primary electron can be pictured as a tube of about 2 x 10^{-5} cm diameter [13], filled by electrons and positive ions. The charge density along the axis of the tube increases monotonically until the end of the electron track. Side tracks of low energy delta electrons with high ionization yields are also produced. Recombination is strongest on these tracks and larger fluctuations in the number of charges collected from these delta electron tracks have to be expected, as suggested by Bolotnikov *et al.*

In order to account for this effect we have fitted the same data with the function:

$$Q = (Q_0-Q_\delta)/(1+k/E) + Q_\delta/(1+k_\delta/E), \qquad (2)$$

where Q_δ is the charge produced by delta electrons and k_δ is the recombination constant corresponding to this charge. Clearly the recombination constant k associated with the primary track has a different value than the one derived from Eq. (1).

Delta electrons of all energies from the W-value up to the energy of the primary electron, can be produced by ionization, although the probability decreases rapidly with energy. At extremely low energies a delta electron cannot produce enough electron-ion pairs to increase the charge density and thus the recombination. At high energies delta electron tracks will resemble the primary track, and again the recombination rate will not be different. For some energy interval in between, however, the necessary conditions for increased recombination are fulfilled. In Eq. (2) Q_δ represents the charge liberated by exactly these delta electrons, without specifying the boundaries of the energy interval. All the charge from delta electrons outside this energy interval cannot be distinguished from that of the primary track and therefore contribute to Q_0 rather than Q_δ. In reality a different Q_δ and k_δ should be associated with each delta electron track of a given energy. Eq. (2) is therefore only an approximation with the two delta electron parameters to be considered as weighted averages on all possible delta electron energies.

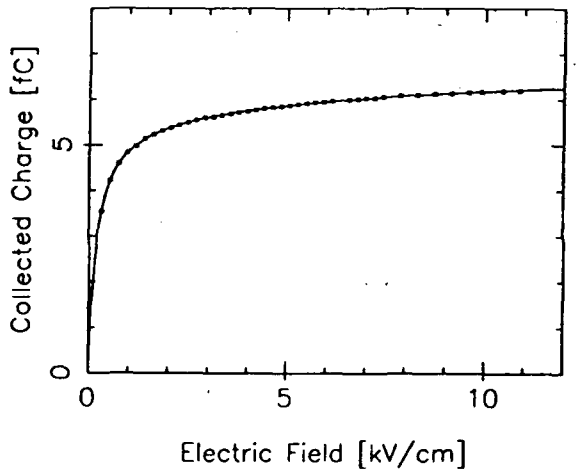

Fig. 3. Field Dependence of the Charge Collected for the 976 keV Electrons. The line is a fit to the points with Eq. (2). The values of the fitted parameters are: $Q_0 - Q_\delta = 5.68 \pm 0.04$ fC, $k = 0.2 \pm 0.03$ kV cm^{-1}, $Q_\delta = 1.28 \pm 0.15$ fC, $k_\delta = 12 \pm 3$ kV cm^{-1}, and $\chi^2 = 0.2$ per degree of freedom.

Fig. 3 shows the fit of Eq. (2) to our 976 keV data. The values of the four parameters and the normalized χ^2 are also given. The quality of the fit is much better than would be expected from a simple increase in the number of parameters from two to four. While the contribution to the total collected charge from the primary electron track saturates very early, the part of the signal due to delta electrons rises slowly up to extreme fields. At a field $E = k_\delta$ only 50% of Q_δ is collected. Because of this slow increase with field, the determination of k_δ and Q_δ from our data, which are limited to about 11 kV cm^{-1}, cannot be very accurate.

From this analysis we conclude that about 20% of the total ionization produced by a 976 keV electron in liquid argon is deposited in form of delta electrons. At our maximum field strength, more than 50% of this charge is lost through recombination.

We have calculated the expected number dn_δ of delta electrons per centimeter with energies in the interval between E_δ and $E_\delta + dE_\delta$, produced by a 976 keV electron in liquid argon. Using the formula based on Mott's cross section for the elastic scattering of electrons by the Coulomb field of a nucleus and neglecting relativistic corrections we have:

$$dn_\delta = (2\pi N e^4/m_e v^2)(dE_\delta/E_\delta^2) \qquad (3)$$

with N the number of electrons per cm^3 of argon, v the velocity of the scattering electron, E_δ and m_e the kinetic energy and mass of the delta electrons. The track length of a 976 keV electron in liquid argon has been divided in very small steps and in each step the probability to create delta electrons within a given energy interval has been calculated with Eq. (3). Fig. 4 shows the average amount of energy lost by the primary particle for the production of delta electrons with energies below 50 keV. Only those delta electrons for which recombination is significantly enhanced with respect to the primary particle have to be considered in this calculation. As explained before, a lower and upper limit in energy should be established to define this special class of delta electrons. Following the considerations of Miroshinicenko *et al.* [14], we choose the energy range between 1 and 20 keV for the delta electrons which exibit a significantly different ionization density. In this range about 200 keV of the primary electron energy are lost in form of delta electrons, which matches the 20% obtained from our data. However, the result of the calculation depends critically on the chosen energy limits and can only be viewed as a rough estimate.

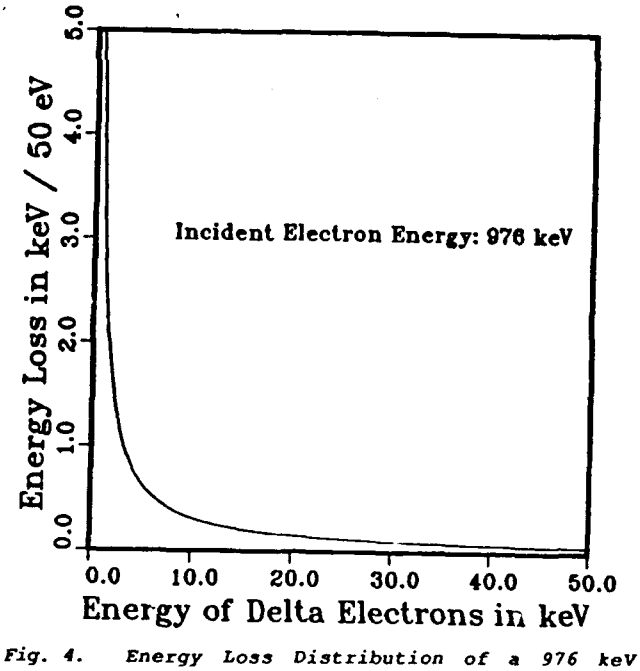

Fig. 4. Energy Loss Distribution of a 976 keV electron for Production of delta electrons of Energies up to 50 keV.

3.2. Energy Resolution

The energy resolution is determined by statistical fluctuations in the total charge collected. The ionization electrons produced along the primary track are nearly all detected. The fluctuations in their number should therefore be well described by the Fano factor (F = 0.11). Much larger fluctuations are expected in the number of charges

from delta electrons. If F_δ is the equivalent of the Fano factor for this part of the signal, we expect that at fields much higher than the value of k_δ, fluctuations in Q_δ should be described by a $F_\delta = F$, while at very low fields Poisson statistics should hold ($F_\delta = 1$), since most of the electrons are lost through recombination.

In first approximation the expected resolution can therefore be written as:

$$\Delta E/E = 2.35 q_e^{1/2} [(F(1+k/E)/(Q_0-Q_\delta) + (F_\delta/Q_\delta)(1+k_\delta/E)]^{1/2}, \qquad (4)$$

where q_e is the electron charge and F_δ has a value between 0.11 and 1. Fig. 5 shows the noise subtracted energy resolution for the 976 keV electron line as measured in our liquid argon chamber, as a function of drift field. The errors on the widths of the measured lines ar much larger than those on the mean values. Typical error bars are shown at three different field strengths.

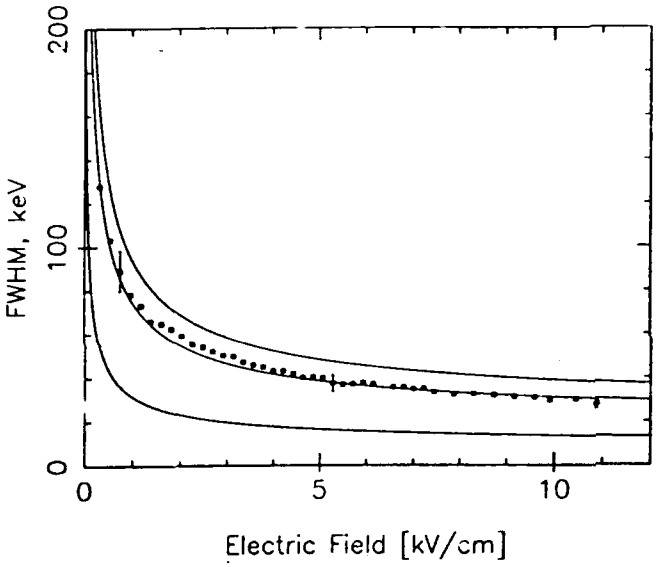

Fig. 5. Field Dependence of the Noise Subtracted Energy Resolution of 976 keV Electrons in Liquid Argon. The line through the points is the best fit of Eq. (4) with an $F_\delta = 0.62$. The upper and lower lines show the predictions of Eq. (4) in the cases where the fluctuations in the charge from delta electrons are described by an $F_\delta = 1$ (Poisson statistics) or $F_\delta = 0.11$ (Fano statistics), respectively.

The measured points fall in between the two limiting cases of $F_\delta = 0.11$ and $F_\delta = 1$ indicated by the two outer solid lines. For an $F_\delta = 0.62$ Eq. (4) agrees fairly well with the data.

Better resolution is achievable if the ionization chamber is operated at a much higher drift field than the maximum reached in the present study.

3.3. Effect of Xenon Doping

The field dependence of the charge and energy resolution of ^{207}Bi electrons was also measured in liquid argon doped with 1% xenon. The xenon was admixed in the gas phase. We assume that its concentration in the liquid did not change significantly. Fig. 6 shows a typical pulse-height spectrum of ^{207}Bi electrons with and without xenon. The dominant 976 keV peak is clearly higher in the mixture than in the pure liquid. The tests were repeated twice using the same gas mixture, and results were reproducible. The increase in charge collection relative to pure liquid argon was about 13%, constant within errors at all drift fields, as shown in Fig. 7.

The enhanced ionization from xenon doping is explained by the existence of exciton states in liquid argon, first confirmed by Kubota *et al.* [15]. Xenon can be ionized by these excited states which have higher energies than the ionization potential of xenon in liquid argon (10.58 eV).

In terms of energy resolution one would expect an improvement in xenon doped argon, due to the smaller Fano factor calculated for this mixture [1]. Our data however, show no difference in energy resolution compared to pure liquid argon. This is consistent with the hypothesis that recombination on low energy delta electrons limits the resolution of ionization chambers much more than the Fano factor, as previously discussed.

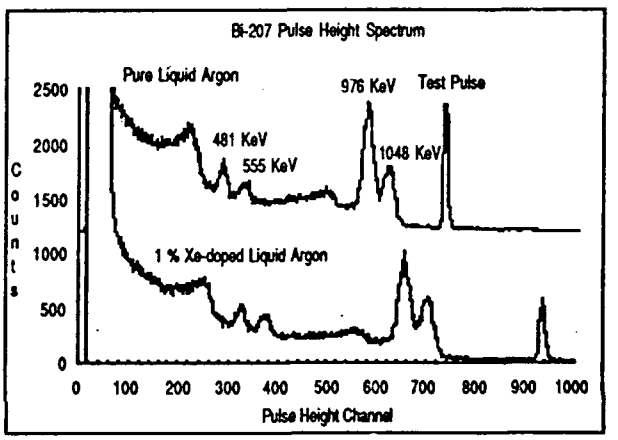

Fig. 6. Comparison of the ^{207}Bi Pulse Height Spectrum in Liquid Xenon-Doped Argon and in Pure Liquid Argon. The drift field is 8.3 kV cm^{-1}.

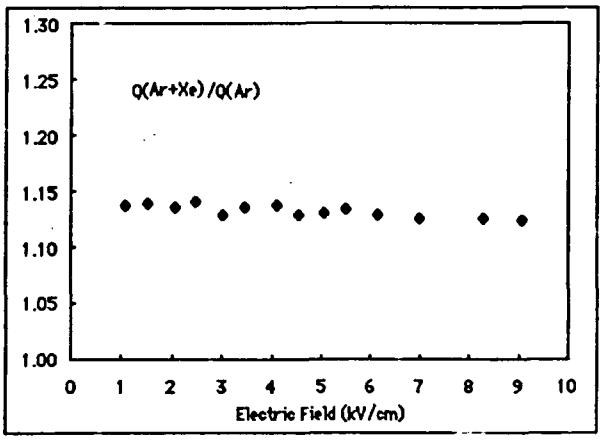

Fig. 7. Field Dependence of the Ionization of 976 keV Conversion Electrons in Xenon-Doped Liquid Argon Relative to Pure Argon.

4. Conclusions

The electric field dependence of the energy resolution measured in a liquid argon ionization chamber has been analyzed by taking into account the production of highly ionizing delta electrons. Following an interpretation by Bolotnikov *et al.* of their measurements with high pressure xenon, we have fitted the saturation curve in liquid argon assuming a different recombination rate on the part of the

signal produced by delta electrons. The data show that about 20% of the collected charge is associated with delta electron tracks. At the maximum field used in our study we collect less than 50% of this charge. The dependence predicted for the energy resolution on the drift field agree well with the data if an average value of 0.62 is assumed to describe the fluctuations on the charge collected from delta electrons. We conclude that the best experimental values for the resolution measured so far in liquid argon are consistent with the expectations at those fields.

The ultimate Fano limit should be reached if all recombination effects are overcome. To limit recombination and hence improve the energy resolution one has to increase the electric field or, alternatively, increase the electron mobility, for example by cooling the argon to liquid helium temperature. On the other hand part of the scintillation light produced in liquid argon is associated with the recombination process. One can therefore minimize the charge loss by directly detecting the ultraviolet photons signal and add it to the electron one. Another alternative is to add a photosensitive dopant to the liquid to convert the scintillation light into detected charges.

Finally, our data in argon doped with 1% xenon confirm an enhanced ionization yield due to the existence of exciton states in liquid argon, but do not show any improvement in the resolution despite the smaller Fano factor calculated for this mixture. This could be consistent with the dominating effect of delta electrons.

We would like to thank Adrienne M. Cool for her dedication and valuable assistance during these tests. This work was supported by a grant from DARPA (#N-00014-86-C-0086).

References

[1] T. Doke, A. Hitachi, S. Kubota, A. Nakamoto and T. Takahashi, *Nucl. Instr. Meth.* 134, 353 (1976).

[2] T. Doke, *Portgal. Phys.* 12, 9 (1981).

[3] I. M. Obodovsky and S. G. Pokachalor, *Low Temp. Phys.* 5, 829 (1979).

[4] M. D. Edmiston and C. R. Gruhn, *IEEE Trans. Nucl. Sci.* NS-25, 352 (1978).

[5] T. Lindblad, L. Bagge, A. Engstrom, J. Bialkowski, C. Gruhn, W. Pang, M. Roach, and R. Loveman, *Nucl. Instr. Meth.* 215, 183 (1983).

[6] E. Aprile, W. H.-M. Ku, J. Park, and H. Schwartz, accepted for publication in *Nucl. Instr. Meth.* (June 1987).

[7] A. E. Bolotnikov, V. V. Dmitrenko, A. S. Romanyuk, S. I. Suchkov, Z. M. Uteshev, *Pribory i Tekhnika Eksperimenta* 4, 42 (1986).

[8] E. Aprile, K.L. Giboni and C. Rubbia, *Nucl. Instr. Meth.* 241, 62 (1985).

[9] *Argon, Helium and the Rare Gases, Vol. I*, 227 (1961).

[10] Model 1000 Gas Purifier, SAES Getters, Milano, Italy.

[11] G. Jaffe, *Ann. Phys.* 42, 303 (1913).

[12] H.A. Kramers, *Physica* 18, 665 (1952).

[13] S. Kubota, M. Hishida, M. Suzuki, and J. R. (Gen), *Phys. Rev.* B20, 3486 (1979).

[14] V. P. Miroshnicenko, P. L. Newskij, B. U. Rodionov, *Proceedings of the Conference on Elementary Particles and Cosmic Rays*, Moskow, Energoizdat (1982).

[15] S. Kubota, A. Nakamoto, T. Takahashi, S. Konno, T. Hamade, M. Miyajima, A. Hitachi, E. Shibamura, and T. Doke, *Phys. Rev.* B13, 1649 (1976).

†Present address: Citicorp, 670 Maryon Ridge Center Drive, MS 75, St. Louis, Missouri 63141

DEVELOPMENT OF LIQUID XENON DETECTORS FOR GAMMA RAY ASTRONOMY

Elena Aprile
Masayo Suzuki

Reprinted from
IEEE TRANSACTIONS ON NUCLEAR SCIENCE
Vol. 36, No. 1, 1989

DEVELOPMENT OF LIQUID XENON DETECTORS FOR GAMMA RAY ASTRONOMY

Elena Aprile and Masayo Suzuki

Physics Department and Astrophysics Laboratory
Columbia University
New York, New York 10027

ABSTRACT

The application of liquid xenon in high resolution detectors for gamma ray astronomy is being investigated. Initial results from a pulse shape analysis of ionization signals in a liquid xenon gridded chamber indicate that we are able to achieve the necessary liquid purity for the transport of free electrons with simple techniques. The energy resolution has been measured as a function of applied electric field, using electrons and γ-rays from a ^{207}Bi source. At a field of 12 kV/cm the noise subtracted energy resolution of the dominant 569 keV γ-ray line is 34 keV FWHM. This value, which is the best reported to date in liquid xenon at similar field strengths, is mostly determined by recombination of electron-ion pairs on delta-electron tracks.

1. INTRODUCTION

Instruments which combine high detection efficiency with good spectral and spatial resolution and a large effective area are required to make significant advances in gamma ray astronomy. A liquid xenon ionization chamber can potentially fulfill these requirements. The sensitivity for the detection of weak gamma ray sources in space in the energy range between 100 keV and several MeV can be improved by orders of magnitude over currently used germanium and sodium iodide spectrometers. The possibility of 3-dimensional track imaging in a liquid xenon time projection chamber, triggered by the primary scintillation light, will add a unique capability for background identification and reduction.

According to these considerations, we have performed several experiments with liquid xenon, measuring both ionization and scintillation yields with various radiation sources. Here we present some of the results on the two basic issues of purity and energy resolution.

The purity level of the liquid remains the crucial prerequisite for the successful operation of an ionization device since it affects directly the total charge collected and, therefore, the energy resolution. Serious difficulties have often been experienced with the purification of xenon, compared to the more commonly used and much less expensive liquid argon, for which effective purification procedures have been well demonstrated [1-3]. Liquid xenon has a much higher boiling point which allows more impurities to remain in solution. In addition, the cross section for electron attachment by oxygen molecules is larger in xenon than in argon [4].

Compared to the high expectations for energy resolution in liquid xenon, based on the small calculated Fano factor [5], the experimental results have been rather poor [6-10]. We have repeated these measurements with electrons and γ-rays, as well as with heavily ionizing alpha particles, in order to understand the basic limiting processes.

While the reasons for the discrepancy between theory and experiment have often been related to experimental limitations of the detection systems, we find it hard to believe given the consistency of the results obtained with entirely different purification and detector systems. We suggest that at the moderate field strengths typically applied, complete charge collection is not achieved due to strong recombination effects on the tracks of low energy delta electrons accompanying the primary ionizing track. We have already demonstrated that this delta electron hypothesis explains well energy resolution data in liquid argon [11]. Similar conclusions have been recently reported by other authors [12,13]. An analysis of the liquid xenon ionization data, which takes into account the effects of delta electrons production, is in progress.

2. EXPERIMENTAL APPARATUS

2.1 *Ionization Chambers*

The gridded ionization chambers used for the measurements with liquid xenon were similar to those described in detail in two previous publications on liquid argon results [3,11].

The energy resolution was determined in a gridded ionization chamber with 2.4 mm between grid and cathode and 2 mm between anode and grid. The electroformed nickel mesh used as grid had a 1% shielding inefficiency and a 100% transmission for a 2 to 1 ratio of collection to drift field. A higher field ratio was however used for the measurements.

A ^{207}Bi source electroplated on the cathode center was used to irradiate the chamber. Two independent, RC filtered power supplies provided the negative voltages on the cathode and on the grid. The anode was directly coupled to the input of a charge sensitive preamplifier. The charge signal was passed through a spectroscopy amplifier (Ortec 450) before being fed into a multichannel analyzer (ND-65). Bipolar shaping with 3μsec time constants was used. Typical RMS noise of the electronic system was on the order of 300 electrons. A test pulse coupled with a 1 pF capacitor to the gate of the input FET served for charge calibration. We estimate a minimum of 10% systematic error on the absolute charge measurement.

The purity of the liquid xenon was measured with cosmic ray tracks traversing a chamber with the cathode-grid spacing enlarged to 30 mm. A field shaping ring halfway between cathode and grid was necessary to avoid field inhomogeneities at the edges of the active volume. The anode-grid separation was kept at 2 mm. The voltages to grid, cathode and ring were independently supplied. The shape of the ionization signals produced in the chamber were analyzed at the output of the integrating preamplifier. The decay time constant was set to 1 msec to allow detection of very long electron lifetimes, longer than 100μsec. A digital oscilloscope (Tektronix 2430) digitized the waveforms. It was interfaced via a GPIB bus to

0018-9499/89/0200-0311$01.00 © 1989 IEEE

a Macintosh computer for data handling and storage.

2.2 *Purification System*

Impurities in the xenon may come from the gas composition itself, from outgassing of construction materials and from external leaks. The best grade of commercially available xenon gas is not sufficiently pure for the operation of an ionization chamber. The level of O_2 is in range of 1 part in 10^6 (1ppm), and so are other electronegative substances like CO_2 and H_2O. The level of N_2 is of the same order, but the attachment of electrons to nitrogen is between 10^2 and 10^4 weaker than the attachment to oxygen. Several hundred ppb of hydrocarbons and fluorocarbons are also present and must be removed. We have purified xenon in the gas phase, using a combination of chemical and passive absorbers. The system is schematically shown in Fig. 1.

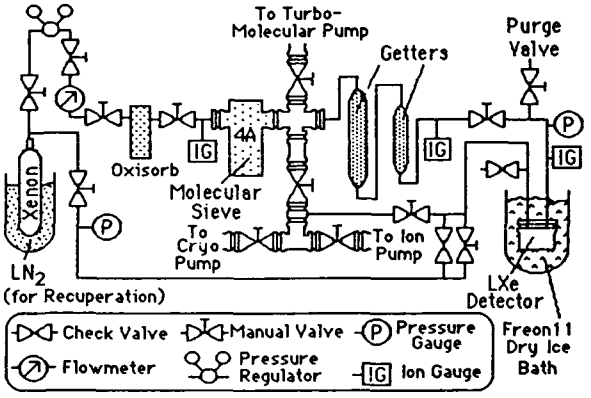

Figure 1. Layout of the xenon gas purification system.

The gas is first passed through an Oxisorb cartridge which reduces the oxygen level to the 5 - 10 ppb range and also reacts with other gases such as CO_2 and H_2O. The molecular sieve trap (4A type), which follows the Oxisorb, strongly adsorbs water and hydrocarbons. We renounced to the use of the 13X type molecular sieve in conjunction with the 4A type since xenon is easily absorbed in this zeolite. The high temperature getters in the final stage should lower the concentration of impurities below the desired 1 ppb level.

The xenon gas purified in this sequence is then condensed in the test chamber by surrounding it with freon at dry ice temperature in an open bath. After each measurement the xenon from the chamber is recollected into the original stainless steel gas cylinder kept at LN_2 temperature.

The whole system was baked under vacuum for several weeks after initial cleaning and assembly, and was always kept under vacuum in between measurements. The molecular sieves were regenerated by baking at 300°C under a vacuum of about 10^{-7} Torr. Typical outgassing rate of the system was better than 10^{-8} Torr liter/sec.

The getter was a commercially available unit (SAES 1000R) containing an alloy of (Zr-V-Fe). After the activation, achieved by heating the getter under vacuum for a period of about an hour, the passage of the gas would start. The flow rate was on the order of 1.5 liters/min. The getter temperature during filling was 500°C. While oxygen, carbon and nitrogen atoms, once chemisorbed, cannot be released again due to the formation of strong chemical bonds with the alloy atoms, hydrogen atoms absorbed at lower temperatures can be released when heated. At the end of the activation period we measured a pressure rise from 10^{-7} Torr to about 10^{-6}, which we attribute to the hydrogen diffusing out of the getter. To reduce the concentration of hydrogen and the eventual formation of hydrides in the chamber volume, we introduced a second getter (SAES 250N) composed of Zr-Fe and operated at much lower temperature (150°C) A comparison of energy resolution data obtained with or without the second getter in the purification system shows no substantial improvement.

The same xenon sample was used to fill both chambers, the one to determine the energy resolution, and the other one to measure the liquid purity. Before filling, the chambers were kept at a temperature of 150°C or higher, when possible, under a vacuum of better than 10^{-6} Torr for a period of at least 24 h. Typical outgassing rates were on the order of 10^{-9} Torr liter/sec.

2.3 *Cryogenics*

At atmospheric pressure, the liquid phase of xenon extends from approximately 162 K to 165 K, so that a precisely temperature controlled cooling unit is mandatory. Typically, liquid nitrogen vapors are used for liquefying xenon. We have chosen a more practical cooling system for laboratory tests of small scale prototypes. A bath of Freon-11 (CCl_3F) mixed with dry ice surrounds the detector, providing an easy and reliable way to maintain the temperature at 195 K, the sublimation point of CO_2. Since the vapor pressure of xenon at this temperature is about 3.5 atm, the pressure of the gas has to exceed this value to condense (Fig. 2).

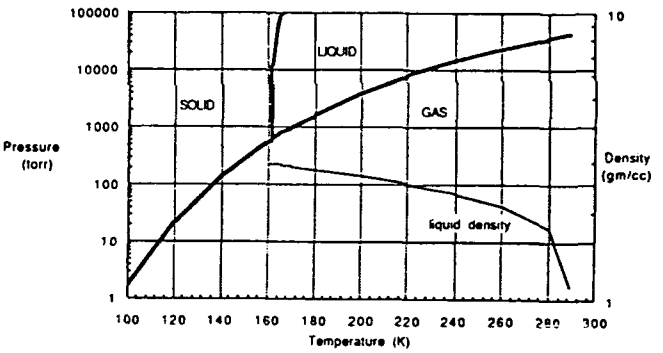

Figure 2. Xenon phase diagram and liquid density dependence on temperature.

We typically filled the gas with about 5 atm through the purifiers. Operating at dry ice temperature rather than the normal boiling point, reduces the density of the liquid from about 3.1 g/cm^3 to 2.8 g/cm^3. Another consequence of the higher temperature is an increase of the electron mobility from typical values around 1000 cm^2/Vs at a temperature close to the triple point (161.3 K) to values around 4000 cm^2/Vs at 200 K [14,15]. The high electron mobility expected at our operating temperature was confirmed from the purity test data [16].

3. RESULTS AND DISCUSSION

3.1 *Purity Measurements*

Attachment of free ionization electrons to electronegative impurities is one of the processes which reduces the total collected charge and, thus, the energy resolution of an ionization chamber. The result of attachment is the conversion of a highly mobile electron into a negative ion which is too slow to con-

tribute to the electronic signal. The shape of this signal is modified by the presence of impurities and can be approximately described by the function

$$Q(t) = Ne(\tau/t_d)(1 - \exp(-t/\tau)) \quad (1)$$

where Ne is the total charge left in the drift region after initial recombination, t_d is the drift time and τ is the attenuation time or so-called electron lifetime.

The most direct way to test the liquid purity in an ionization chamber is to measure the lifetime of the electrons before capture by electronegative impurities. The drift time of the electrons in the grid-cathode region must be of the same order as the electron lifetime. In a chamber of practical size, i.e. with limited drift length, the maximum drift time can be prolonged to the right range in order to measure the effect with sufficient accuracy by reducing the electric field strength and, consequently, the drift velocity to very low values.

We recorded the shape of ionization signals from cosmic ray tracks traversing the purity chamber for a wide range of field strengths, from 5 V/cm to 500 V/cm. Two typical pulses at 8 V/cm and 150 V/cm are shown in Fig. 3 as recorded with the digital oscilloscope.

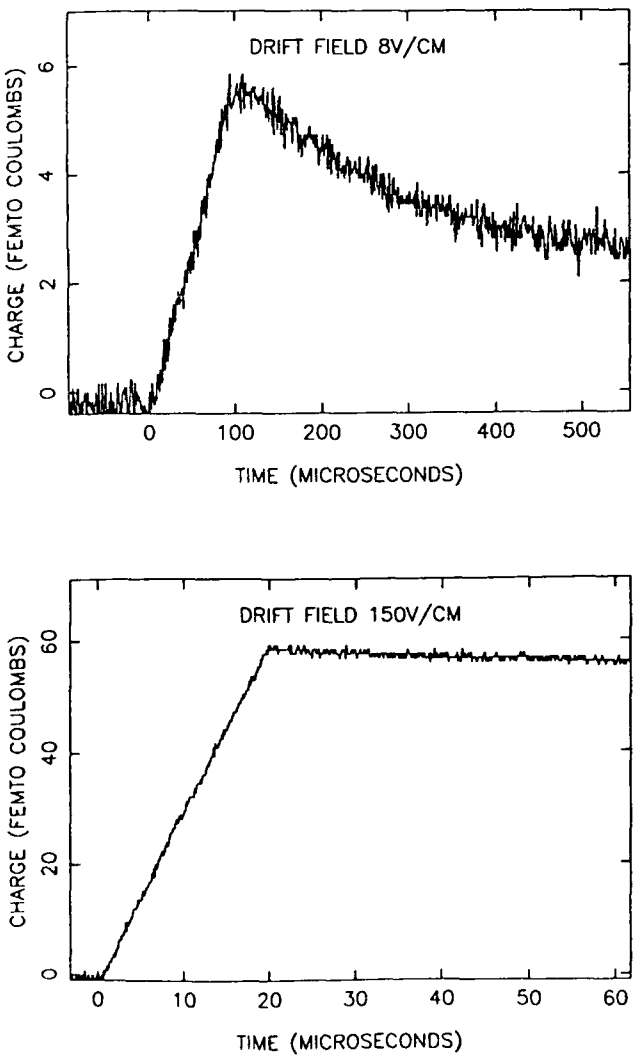

Figure 3. Single ionization pulses in liquid xenon at 8 V/cm and 150 V/cm

The rise of the pulse at 8 V/cm is still approximately straight. Below this field the signal pulse height decreases substantially and the rounding of the pulses increases, indicating a clear effect of attachment.

The analysis of these pulse shapes is still in progress and results on attenuation time as well as on drift velocity and low field electron mobility at 195 K will be presented in a forthcoming paper [16].

For a preliminary estimate of the impurity concentration in our liquid xenon sample we determined that the electron lifetime is at least 100 msec, the maximum drift time measured at 8 V/cm.

The concentration $[s]$ of oxygen equivalent substances is related to τ by :

$$\tau = 1/k_s[s] \quad (2)$$

where k_s is the attachment rate constant in liter/moles/sec. The measured value for k_s in liquid xenon at 165 K is on the order of 2×10^{11} liter/moles/sec at a field of 10 V/cm [4]. The concentration ρ in ppb is related to $[s]$ by:

$$\rho = [s]/n_{Xe} \quad (3)$$

where n_{Xe} is the number of moles in one liter of liquid xenon. From the value of $[s]$ obtained from equ. (2) and $n_{Xe} = 21$ we deduce:

$$\rho \sim 0.3 \text{ ppb} \quad (4)$$

This estimate applies to the concentration of oxygen like substances, but it is also indicative of the concentration of N_2O which has an attachment rate constant similar to that of oxygen at low fields. However, while attachment to O_2 molecules decreases with increasing field, attachment to N_2O increases by more than an order of magnitude [4].

Since one has to operate at relatively high fields to minimize the recombination process, it is important to identify impurities which, similarly to N_2O, may have attachment cross sections strongly dependent on the electric field. These considerations indicate the importance of substances other than O_2 as electron trapping impurities in liquid xenon, and the need for more studies in this direction.

3.2 *Energy Resolution Measurements*

Fig. 4 shows typical ^{207}Bi energy spectra measured at different electric fields in liquid xenon. These data were obtained in our initial tests with liquid xenon using the chamber geometry described earlier and with only one getter in the purification sequence. Data have been accumulated in several successive runs, with different electrode spacings and different operating conditions of the purifiers. All results are consistent, within errors, with the ones displayed in Fig. 4. The contribution of the electronic noise in this run was on the order of 16 keV FWHM.

The total data set available covers a wide range of fields between 50 V/cm and 12 kV/cm. Measurements at higher fields, limited so far by electrical breakdowns, are underway with a modified chamber design. The ^{207}Bi spectra in liquid xenon are quite different from those observed in liquid argon [3]. Due to the high efficiency of xenon for γ-rays, the pulse height distribution is dominated by the full energy peaks of γ-rays at 569 keV and 1064 keV. This last γ-ray line includes counts from conversion electrons of 1048 keV. The Compton edges are also identified. The internal conversion electrons of energy 481 keV and 976 keV, which dominate the ^{207}Bi spectrum in liquid argon, are now less visible until

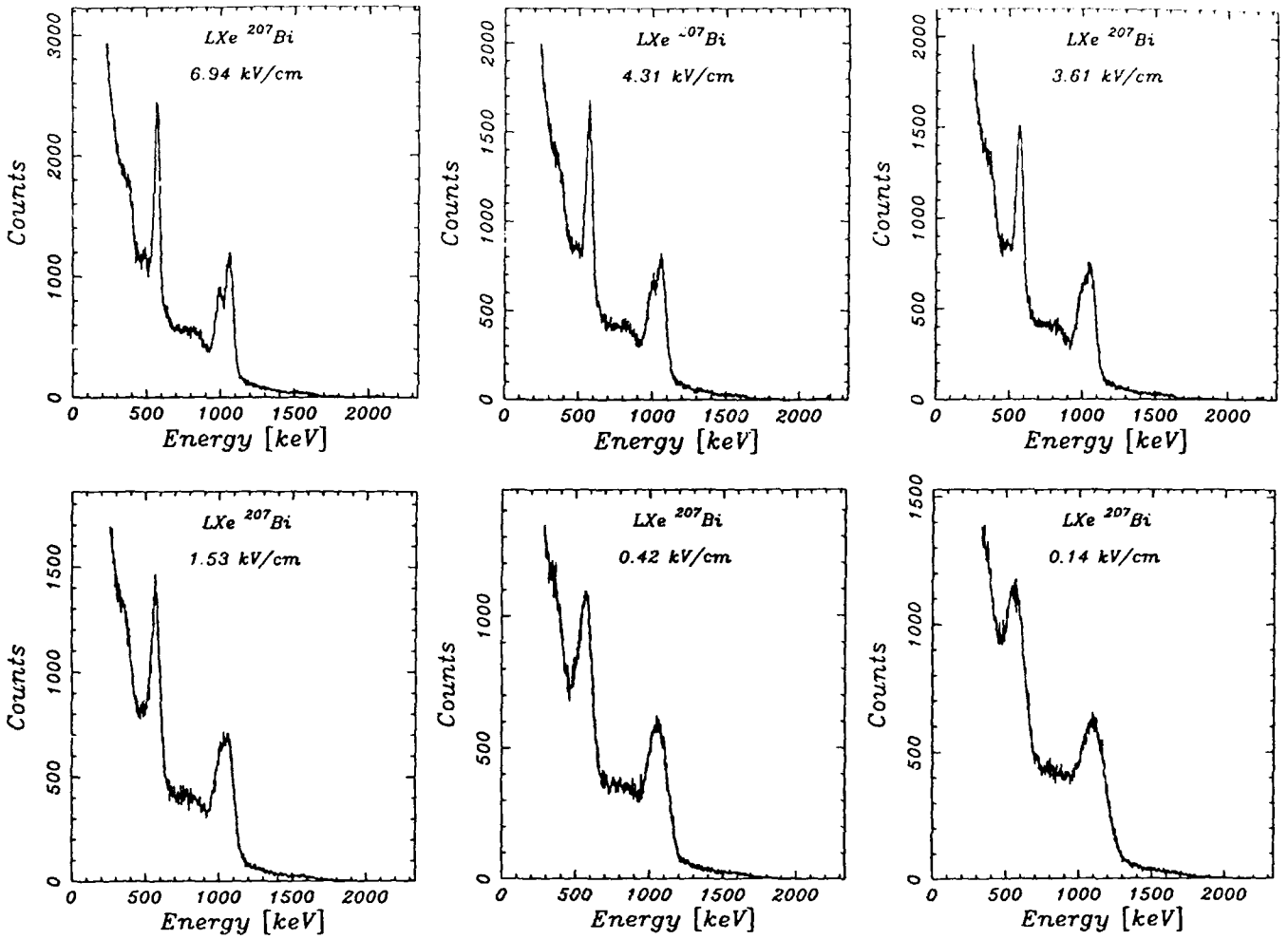

Figure 4. Electric field dependence of the ^{207}Bi pulse height distribution in liquid xenon. The typical electronic noise contribution to these data was 16 keV (FWHM).

fields above 4 kV/cm are applied. A least square fit of Gaussians to the electron and γ-ray peaks at the highest field of 12 kV/cm yields a total energy resolution of 43 keV and 55 keV FWHM for the 569 keV and 1064 γ-rays, respectively (Fig. 5). The electronic noise contribution in this particular spectrum is 26 keV FWHM, as indicated by the fitted test pulse distribution. The subtraction in quadrature of this noise level gives 34 keV and 48 keV FWHM for the two gamma ray peaks.

These are the best values measured so far in liquid xenon at similar fields. It is however clear, by carefully comparing all the best energy resolution data measured by various groups, with different chambers, purification systems and radiation sources, that the discrepancy between the theoretical Fano limited energy resolution of few keV and the experimental values is too large to be explained with purification problems, geometrical effects, or technical limitations of the apparatus. We believe that in liquid xenon, as in liquid argon, the fundamental process of recombination on low energy delta electron tracks which accompany the primary ionizing particle, is mostly responsible for the observed resolution at the limited electric fields applied.

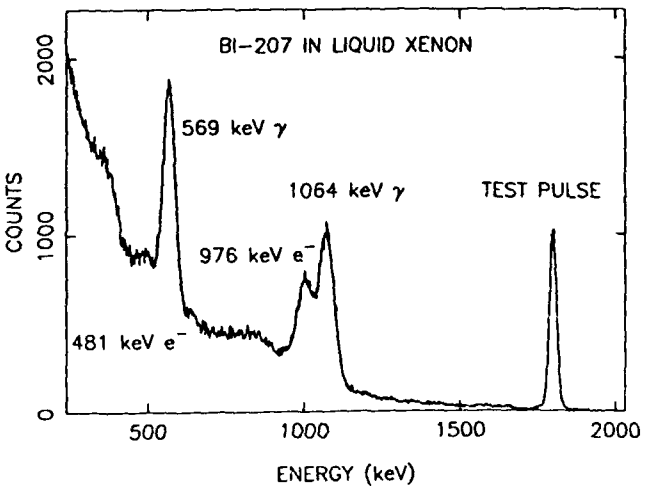

Figure 5. ^{207}Bi energy spectrum in liquid xenon at a field of 12 kV/cm. The solid line is the best Gaussian fit to the data. The total energy resolution of the 569 keV γ-rays is 43 keV (FWHM) with 26 keV (FWHM) of electronic noise.

A detailed analysis based on this hypothesis is in progress. Attachment of electrons to electronegative substances other than oxygen might also affect the resolution measured at high fields but to a much lower extent. A better understanding of these processes is necessary if one wants to determine the ultimate energy resolution performance of liquid xenon and other rare gas liquids.

4. CONCLUSIONS

Our initial investigations with liquid xenon have been encouraging towards the application of this material in instruments with enhanced sensitivity for gamma ray spectroscopy. We have demonstrated that the high purity of the liquid, which is the crucial prerequisite for the feasibility of these instruments, can be obtained with simple and commercially available purification techniques.

Results from studies of the energy resolution in liquid xenon ionization detectors are also very promising. The best value that we have measured so far in liquid xenon is 34 keV FWHM for γ-rays of 569 keV. Studies of the fundamental properties of liquid xenon will continue to provide the basic ground for the optimized detector design for the space environment. It is clear that a liquid xenon detector with the 6% energy resolution achieved so far for the detection of 569 keV γ-rays is preferable to a NaI(Tl) scintillation spectrometer for many astrophysical observations.

This research work was supported by DARPA under contract N00014-86-C-0086, and partially by NASA under contract NAGW-1370.

REFERENCES

[1] E. Aprile, K.L. Giboni and C. Rubbia, *Nucl. Instr. Meth.*, **A241**,62 (1985).
[2] P. Doe, R.C. Allen, S.D. Biller, G. Buhler, W. A. Johnson, H. H. Chen, *Nucl. Instr. Meth.*, **258**, 170 (1987).
[3] E. Aprile, W.H.-M. Ku, J. Park, H. Schwartz, *Nucl. Instr. Meth.*, **A261**, 519 (1987).
[4] G. Bakale, U. Sowada and W.F. Schmidt, *J. Phys. Chem.*, **80**, 2556 (1976).
[5] T. Doke, *Portugal. Phys.*, **12**, 9 (1981).
[6] I.M. Obodovskii and S.G. Pokachalov, *Fiz. Nizk. Temp.*, **5**, 829 (1979).
[7] T. Doke, *Nucl. Instr. Meth.*, **196**, 87 (1982).
[8] K. Masuda, A. Hitachi, Y. Roshi, T. Doke, A. Nakamoto. E. Shibamura and T. Takahashi, *Nucl. Instr. Meth.*, **174**, 439 (1980).
[9] Th. Lindblad, L. Bagge, A. Engstrom, J. Bialkowski, C.R. Gruhn, W. Pang, M. Roach and R. Loveman, *Nucl. Instr. Meth.*, **215**,183 (1983).
[10] A.S. Barabash, A.A. Golubev, O.V. Kazachenko, V.M. Lobashev, B.M. Ovchinnikov and B.E. Stern, *Nucl. Instr. Meth.*, **A236**, 69 (1985).
[11] E. Aprile, W. H.-M. Ku, J. Park, *IEEE Trans. Nucl. Sci.*, **35**, 37 (1988).
[12] K.L. Giboni, *Nucl. Instr. Meth.*, **A269**, 554 (1988).
[13] J. Thomas, D. Imel and S. Biller, *CALT-63-501* (1988).
[14] E.M. Guschchin, A.A. Kruglov and I.M. Obodovskii, *Zh. Eksp. Teor. Fiz.*, **82**,1114 (1982).
[15] S.S.-S. Huang and G.R. Freeman, *J. Chem. Phys.* **68(4)**, 1355 (1978).
[16] E. Aprile and M. Suzuki (in preparation for *Nucl. Instr. Meth.*).

CONTRACT DATA REQUIREMENTS LIST
INSTRUCTIONS FOR DISTRIBUTION
ARPA/ONR

MINIMUM DISTRIBUTION OF TECHNICAL REPORTS

ADDRESSEE	DODAAD CODE	NUMBER OF COPIES UNCLASSIFIED/UNLIMITED	NUMBER OF COPIES UNCLASSIFIED/LIMITED AND CLASSIFIED
Director, Advanced Research Projects Agency 1400 Wilson Boulevard Arlington, Virginia 22209 ATTN: ~~Program Management~~ MR. Edward Brown (NMRO)	HX1241	2	2
Scientific Officer MR Jones (ONR)	N00014	3	3
Administrative Contracting Officer	N62927	1	1
Director, Naval Research Laboratory, ATTN: Code 2627 Washington, D. C. 20375	N00173	6	1
Defense Technical Information Center Bldg. 5, Cameron Station Alexandria, Virginia 22314	S47031	12	2

One (1) copy of each technical report resulting from work performed in the area of tactical technology shall be sent to:

	DODAAD CODE
TACTEC Battelle Memorial Institue 505 King Avenue Columbus, Ohio 43201	79986

MINIMUM DISTRIBUTION OF REPORTS WHICH ARE NOT TECHNICAL REPORTS

ADDRESSEE	DODAAD CODE	NUMBER OF COPIES UNCLASSIFIED/UNLIMITED	NUMBER OF COPIES UNCLASSIFIED/LIMITED AND CLASSIFIED
Director, Advanced Research Projects Agency 1400 Wilson Boulevard Arlington, Virginia 22209 ATTN: Program Management	HX1241	2	2
Scientific Officer	N00014	3	3
Administrative Contracting Officer	N62927	1	1

If the Scientific Officer directs, the Contractor shall make additional distribution of technical reports and such other reports as may be specified by the Scientific Officer in accordance with a supplemental distribution list provided by the Scientific Officer.